Review

The Central Role of Imaging in Renal Cell Carcinoma: Insights into Aggressiveness, Histology and Radiomics

Andreu Ivars *, Blanca Paño, Josep Puig, María Fresno, Leonardo Rodriguez, Carmen Sebastià, Carlos Nicolau

Posted Date: 1 May 2026

doi: 10.20944/preprints202605.0012.v1

Keywords: renal cell carcinoma; computed tomography; tumor aggressiveness; histologic subtypes; radiologic–pathologic correlation; ISUP grade; radiomics; quantitative imaging; renal mass

 doi:10.20944/preprints202605.0012.v1

Review

The Central Role of Imaging in Renal Cell Carcinoma: Insights into Aggressiveness, Histology and Radiomics

Andreu Ivars [1,*], Blanca Paño [1], Josep Puig [1], María Fresno [1], Leonardo Rodríguez [2], Carmen Sebastia [1] and Carlos Nicolau [1]

[1] Radiology Department, Clinic Hospital, IDIBAPS, University of Barcelona (UB), 08036 Barcelona, Spain

[2] Pathology Department, Clinic Hospital, IDIBAPS, University of Barcelona (UB), 08036 Barcelona, Spain

* Correspondence: ivars@clinic.cat

Simple Summary

Renal cell carcinoma is a common form of kidney cancer that can range from slow-growing tumors to highly aggressive diseases. Medical doctors rely on imaging to understand these tumors before treatment, and computed tomography (CT) is the most widely used tool because it is fast, accessible, and provides detailed information on tumor characteristics. However, predicting the aggressiveness of a tumor or its type remains challenging. In this review, we summarize current knowledge on how imaging reflects the biological features of renal cancer, including their appearance, underlying tissue patterns, and level of aggressiveness. We also explored new approaches, such as radiomics, which uses advanced computer analysis to extract information from images that cannot be detected by the human eye. By bringing together existing evidence and highlighting future needs, we aim to support the development of more accurate, standardized, and clinically useful methods for characterizing renal cell carcinoma.

Abstract

Renal cell carcinoma encompasses a heterogeneous group of kidney tumors with wide variations in biological behavior, histologic subtype, and clinical aggressiveness. Accurate preoperative characterization is essential for management; however, it remains challenging due to overlapping imaging features and tumor complexity. CT is the most widely used imaging technique for renal mass evaluation, providing broad availability, high spatial resolution, and multiphasic acquisition capabilities. However, its ability to distinguish histologic subtypes and predict tumor aggressiveness remains limited. This review provides an updated overview of renal cell carcinoma epidemiology and evidence supporting CT as an essential imaging modality. It outlines key radiologic features of main histologic subtypes, highlights markers of aggressive behavior, and discusses the relationship between CT findings and the International Society of Urological Pathology (ISUP) grading system. We explore radiomics, summarizing its methodological foundations and applications in characterizing solid renal masses, emphasizing the need for multicenter studies and standardized radiomic workflows to develop accurate, reproducible tools for improving diagnostic accuracy and risk stratification for renal cell carcinoma.

Keywords: renal cell carcinoma; computed tomography; tumor aggressiveness; histologic subtypes; radiologic–pathologic correlation; ISUP grade; radiomics; quantitative imaging; renal mass

1. Introduction

Renal cell carcinoma (RCC) caused nearly half a million new cases worldwide in 2022, mainly in Europe, Oceania, and North America. It mostly affects older adults, peaks between 60-70 years, and shows male predominance. RCC is the sixth most common cancer in males in the United States

 doi:10.20944/preprints202605.0012.v1

and the 14th–15th globally. Some cases are hereditary, but most are sporadic [1]. Its incidence has risen by 1% annually, partly due to widespread cross-sectional imaging, with over half of RCCs incidentally detected during unrelated abdominal imaging. Increased incidental detection of renal tumors is associated with localized disease in asymptomatic patients. Advanced-stage disease often exhibits clinical symptoms or paraneoplastic manifestations. Early diagnosis and therapeutic improvements have reduced mortality [2].

Globally, about 70% of cases are diagnosed at stage I, while 11% have metastatic disease (stage IV) [3]. Stage alone cannot capture the biological lesion heterogeneity, as many incidental tumors show aggressive behavior or unfavorable histology. In fact, RCC is a heterogeneous disease with multiple histological subtypes, molecular and clinical characteristics affecting survival. Clear cell RCC (ccRCC) is the predominant subtype, comprising 75–80% of cases, and is characterized by inactivation of the von Hippel–Lindau (VHL) tumor suppressor pathway. The remaining 20–25% are non–clear cell RCCs, including papillary and chromophobe subtypes, and a few other entities. Chromophobe tumors have the most favorable prognosis, with 5-year survival rates exceeding 80–90% [4]. Papillary tumors show better outcomes than ccRCC, though outcomes are less favorable for type 2 versus type 1 papillary RCC [5]. Prognostic factors include tumor stage, grade, lymph node involvement, necrosis, and sarcomatoid features correlating with recurrence and survival. However, most variables are determined postoperatively, limiting their value for pre-treatment decisions. This emphasizes the need for accurate, non-invasive imaging biomarkers to distinguish clinically significant disease from low-malignant tumors improving prognostic stratification before therapy.

Guidelines from the American College of Radiology and the American Urological Association emphasize the importance of imaging in evaluating renal tumors [6,7] (Table 1). Ultrasound is an initial modality due to availability and safety, differentiating simple cysts and solid lesions. Contrast-enhanced ultrasound (CEUS) improves lesion vascularity and enhancement assessment, especially for patients contraindicated for iodinated or gadolinium-based contrast agents. However, ultrasound is limited in characterizing tumor biology and inadequate for staging. Computed tomography (CT) with multiphasic protocol remains the standard for RCC detection, characterization, and staging. Its high spatial resolution, reproducibility, and availability make CT crucial for surgical planning and disease assessment [3,8,9]. Dual-energy CT (DECT) has emerged as a complementary technique, enabling material-specific imaging and quantitative iodine assessment. By differentiating enhancing solid lesions and non-enhancing cystic masses, DECT may improve incidental renal tumor characterization when multiphasic protocol is unavailable. Nevertheless, its value in routine clinical practice and in biologic risk stratification remains under investigation [10]. Multiparametric MRI integrates morphologic and functional sequences—T1-weighted, T2-weighted, dynamic contrast-enhanced (DCE) imaging and diffusion-weighted imaging (DWI)—to improve discrimination between benign and malignant renal lesions [11,12]. MRI assesses tumor aggressiveness. High-grade ccRCCs show lower apparent diffusion coefficient (ADC) values on DWI, indicating increased cellularity, and reduced wash-in and enhancement indices on DCE imaging compared to low-grade tumors. Quantitative parameters such as the tumor-to-cortex ADC ratio enhance differentiation, with lower ratios consistently associated with high-grade disease [13–15]. Current guidelines, including the American College of Radiology, recommend MRI as a problem-solving modality for indeterminate renal masses and when CT findings are equivocal [8].

Despite strengths, no imaging modalities reliably distinguish benign from malignant solid renal masses or predict histologic subtype and tumor aggressiveness before treatment. These limitations highlight the need for advanced imaging to extract deeper biologic information from routine images [16,17].

Table 1. Principal imaging tools for renal tumor assessment. .

	US / CEUS	CT / DECT	MRI

 doi:10.20944/preprints202605.0012.v1

Protocol	B-mode, Doppler; CEUS with microbubble contrast	Multiphase (non-contrast, corticomedullary, nephrographic, excretory); DECT with iodine quantification, VUE	T1/T2-weighted, DWI, dynamic contrast-enhanced, subtraction, delayed post-contrast
Clinical applications	Initial detection, cyst vs. other lesions, follow-up, CEUS for vascularity and enhancement	Characterization, staging, surgical planning, DECT for enhancement and cyst vs. solid	Indeterminate lesions, venous involvement, subtyping, cystic lesion characterization, follow-up
Advantages	Widely available, no radiation, safe in renal impairment	High sensitivity/specificity, staging, DECT reduces extra imaging and radiation	Superior soft tissue contrast, functional imaging, no radiation, better for venous involvement
Disadvantages	Operator-dependent, limited for complex/indeterminate masses	Radiation, contrast nephrotoxicity, limited for benign vs. malignant, DECT VUE may underestimate attenuation	Gadolinium risk in severe renal dysfunction, less sensitive for calcifications, costly

US – ultrasound; CEUS – contrast-enhanced ultrasound; CT – computed tomography; MRI – magnetic resonance imaging; DWI – diffusion-weighted imaging; DECT – dual energy computed tomography; VUE – virtual unenhanced images .

2. Histologic Subtypes, Tumor Aggressiveness and ISUP Grading in Renal Cell Carcinoma

2.1. Histologic Subtypes and Pathologic Assessment of RCC

RCC encompasses heterogeneous epithelial malignancies with distinct histological, molecular, and clinical features. The principal histologic patterns include clear cell, papillary, chromophobe, collecting duct, and unclassified morphologies. Three dominant subtypes account for most cases: ccRCC, representing 75–80% of tumors; papillary RCC, accounting for 10–15%; and chromophobe RCC, comprising 5% of cases [1,3].

ccRCC shows clear cytoplasm rich in glycogen and lipids, arranged in solid, acinar, or alveolar patterns, with a delicate vascular network. Papillary RCC is characterized by papillary or tubulopapillary architecture with fibrovascular cores and variable cytologic features by subtype. Chromophobe RCC demonstrates large polygonal cells with pale eosinophilic cytoplasm, prominent cell borders, and perinuclear halos, reflecting its origin from collecting duct system intercalated cells [18]. Less common, but clinically aggressive entities, such as collecting duct carcinoma and unclassified RCC, display infiltrative growth patterns and are often diagnosed at advanced stages.

2.2. Histopathologic Features of Tumor Aggressiveness

Beyond histologic subtype, RCC tumor aggressiveness is determined by specific histopathologic features reflecting cellular atypia and dedifferentiation. Key parameters include nuclear morphology, sarcomatoid or rhabdoid differentiation (Figure 1), and necrosis. High-grade tumors show prominent nucleoli, nuclear pleomorphism, and loss of epithelial differentiation.

 doi:10.20944/preprints202605.0012.v1

Sarcomatoid differentiation represents high-grade dedifferentiation in any RCC subtype, characterized by spindle-shaped malignant cells resembling high-grade sarcoma. Rhabdoid differentiation, defined by large cells with eccentric nuclei and prominent eosinophilic cytoplasmic inclusions, signifies extreme cellular atypia. Both features are associated with aggressive clinical behavior, early metastatic spread, and dismal prognosis [19,20].

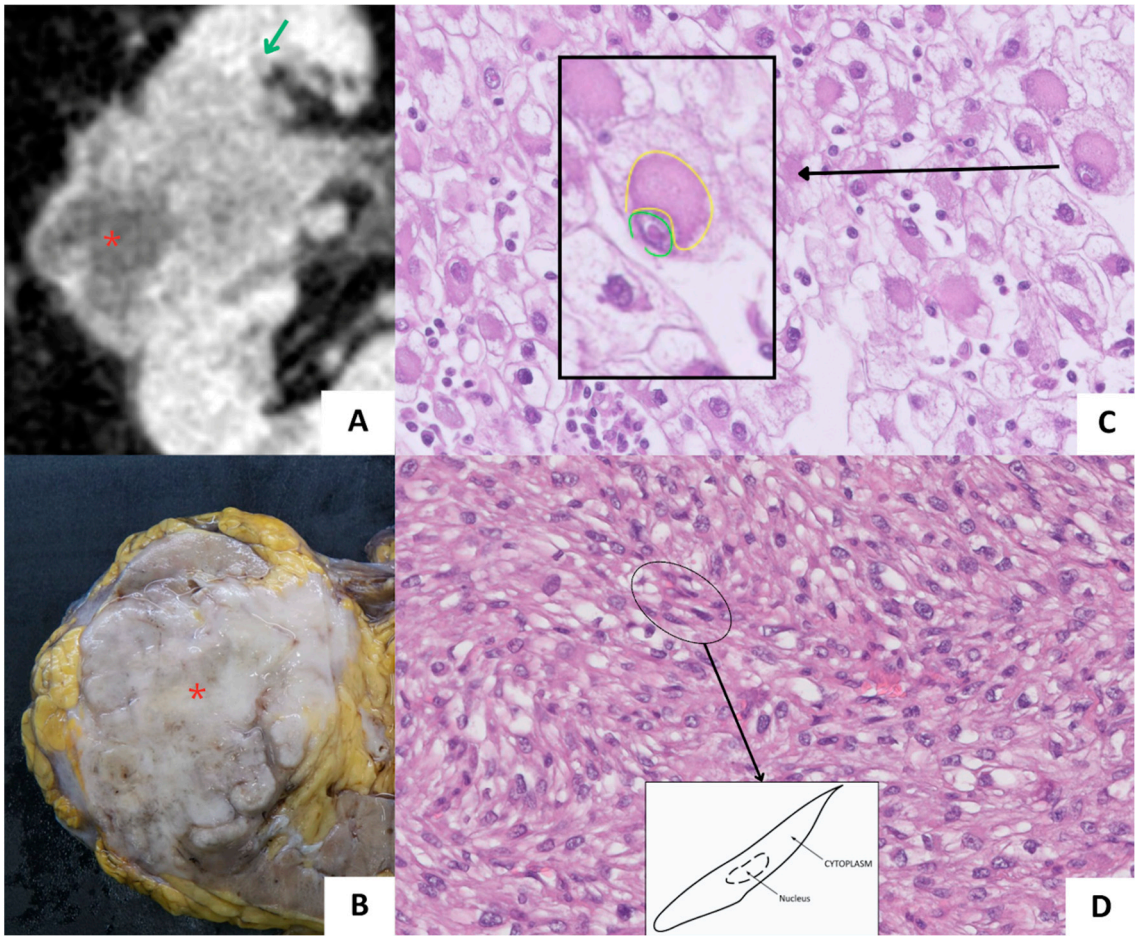

Figure 1. A. Axial CT depicting a solid renal mass (green arrow) with cystic/necrotic area (*). B. Cross section of the gross specimen demonstrating a pale, greyish central area (*) corresponding to necrosis. C. Rhabdoid differentiation. Large epithelioid cell with eccentric nucleus and prominent nucleoli (green oval) as well as abundant eosinophilic cytoplasm (yellow oval). D. Sarcomatoid differentiation. Spindle cells arranged in intersecting fascicles. .

Tumor necrosis (Figure 2) independently predicts survival, mainly in ccRCC [21]. The presence and extent of necrosis reflect rapid tumor growth and hypoxia-driven ischemia and stratifies risk within histologic subtypes and grades. Quantitative necrosis assessment adds prognostic value beyond conventional staging and grading parameters [22].

 doi:10.20944/preprints202605.0012.v1

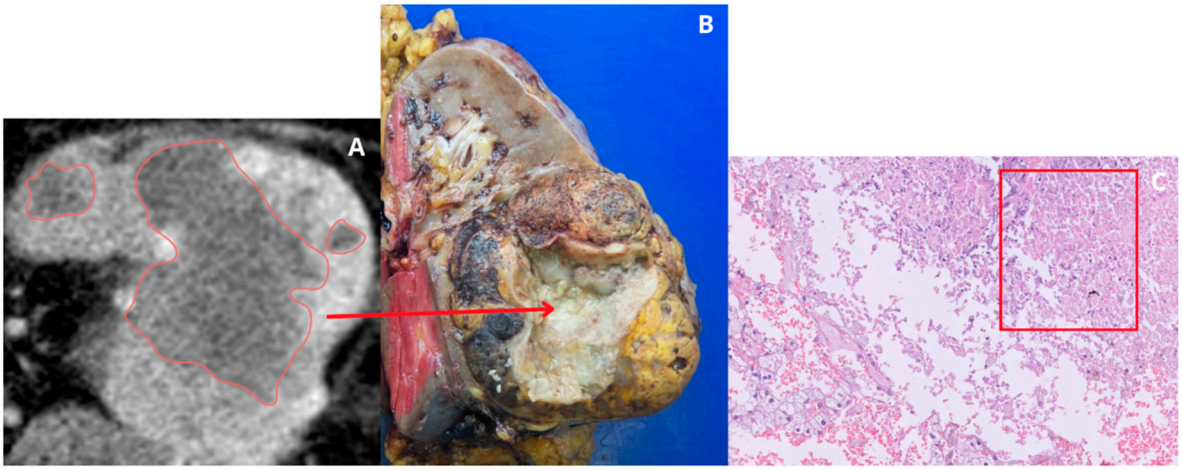

Figure 2. A. Axial CT showing a solid renal mass with hypodense necrotic areas. B. Tumoral necrosis. Cross section of the gross specimen revealing well-demarcated, pale areas. C. Necrotic changes. Amorphous, eosinophilic, granular debris.

2.3. Histopathologic Features of Tumor Aggressiveness

The International Society of Urological Pathology (ISUP) grading system, adopted by the World Health Organization, provides a standardized framework for grading RCC, specifically for clear cell and papillary subtypes. This system is based on nucleolar prominence for grades 1-3 and extreme nuclear atypia or dedifferentiation for grade 4.

ISUP grade 1 (Figure 3) tumors exhibit inconspicuous nucleoli visible at ×400 magnification, whereas grade 2 (Figure 4) tumors demonstrate visible and eosinophilic nucleoli at the same magnification. Grade 3 (Figure 5) tumors have prominent nucleoli identifiable at ×100 magnification. Grade 4 (Figure 6) encompasses tumors with marked nuclear pleomorphism, sarcomatoid differentiation, or rhabdoid features, which supersede nucleolar grading and associate with poor outcomes. The presence of sarcomatoid or rhabdoid differentiation mandates classification as ISUP grade 4, regardless of histologic subtype [23].

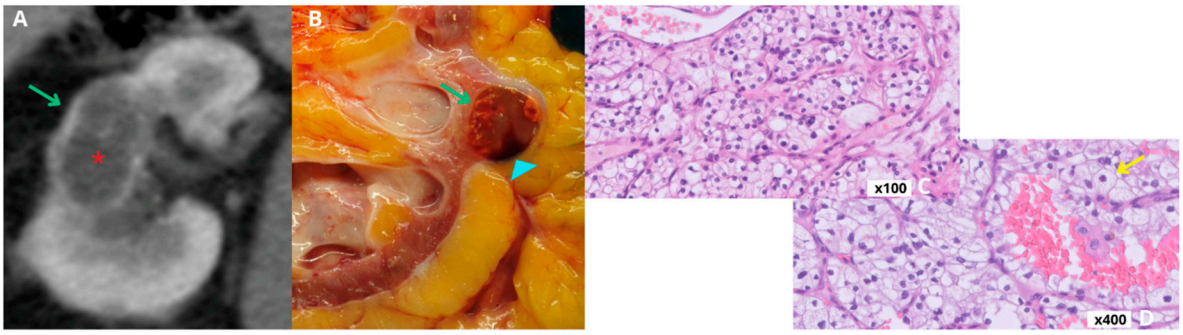

Figure 3. ISUP 1. A. Coronal CT image showing a well-defined ccRCC (green arrow). B. Cross-section of the gross specimen (green arrow). Well-circumscribed renal mass with homogeneous cut surface and cystic hemorrhagic changes (fluid-fluid level; blue arrowhead). C, D. Tumor cells are arranged in acinar pattern, with abundant clear cytoplasm and small oval nuclei. .

 doi:10.20944/preprints202605.0012.v1

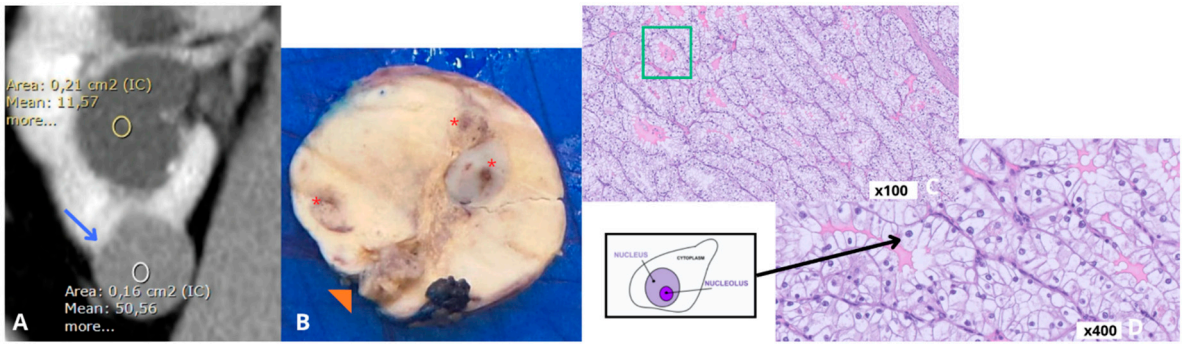

Figure 4. ISUP 2. A. Coronal CT image showing a solid renal tumor with a mean density of 50 HU (blue arrow), and a second lesion, corresponding to a simple cyst. B. Cross-sectional gross specimen showing mildly heterogeneous cut surface (orange arrowhead) and focal hemorrhagic areas (*). C, D. Tumoral cells arranged in acinar pattern with abundant, clear cytoplasm and round/oval nuclei. Nucleoli are visible at x400.

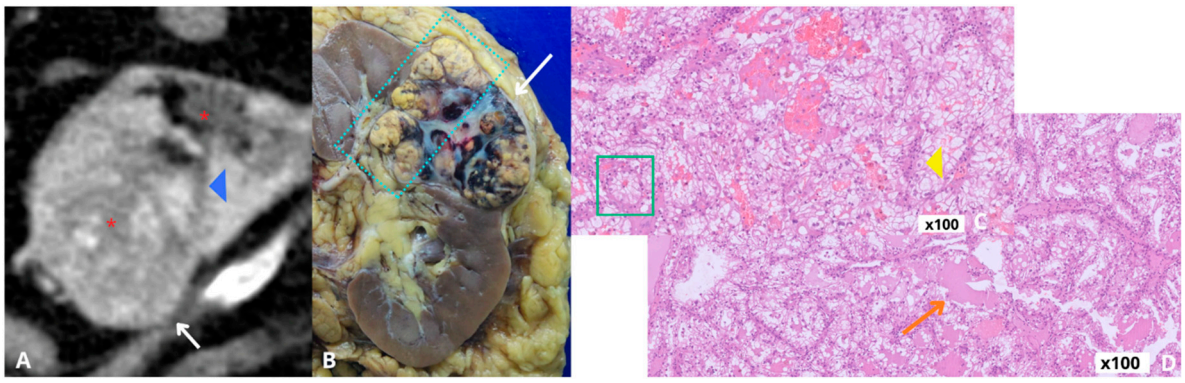

Figure 5. ISUP 3. A. Axial CT image showing a heterogeneous solid renal tumor (white arrow) with ill-defined margins (blue arrowhead) and patchy areas of necrosis (*). B. Cross-section of the gross specimen. Yellow-tan heterogeneous mass with areas of hemorrhage and focal necrosis (white arrow). Capsular rupture along its superior margin and infiltrative borders extending into the perinephric fat and renal sinus (blue rectangle). C, D. Tumoral cells arranged in acinar pattern (C; green square) retaining clear cytoplasm and displaying markedly enlarged nuclei with prominent nucleoli (C; yellow arrowhead). Nuclear pleomorphism and mitotic figures are present, along with patchy areas of coagulative tumor necrosis (D; orange arrow). .

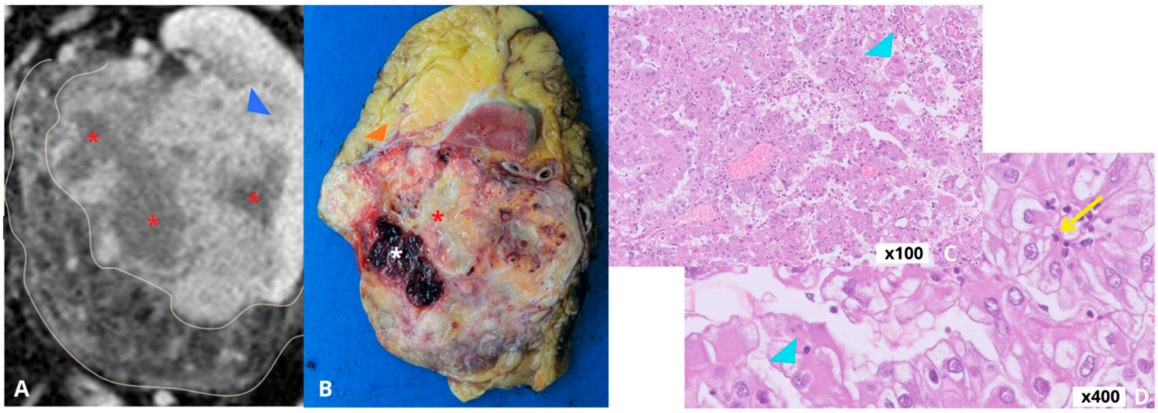

Figure 6. ISUP 4. A. Axial CT image showing a heterogeneous solid lesion with ill-defined margins (blue arrowhead) and large hypodense areas consistent with necrosis (*), as well as extensive stranding of the perirenal fat (yellow curvilineal lines). B. Cross-section of the gross specimen showing a large, poorly circumscribed, heterogeneous mass (orange arrowhead) with infiltrative borders and perinephric fat invasion (orange arrowhead). Variegated cut surface, with gray-white central necrotic foci (*) and hemorrhagic areas (*). C, D.

 doi:10.20944/preprints202605.0012.v1

Extreme nuclear pleomorphism is observed, including bizarre, multilobated, giant tumor cells with prominent nucleoli (D; yellow arrow), along with rhabdoid differentiation (C, D; blue arrowhead).

The ISUP nucleolar grading system is not applied to chromophobe RCC, as it does not reliably demonstrate prognostic value in this subtype [20]. The ISUP grade remains a robust and reproducible prognostic marker for clear cell and papillary RCC and is recommended for routine pathological assessments.

2.4. Clinical Implications on Histologic Grade and Aggressive Features

The integration of ISUP grade with histopathologic features like tumor necrosis and sarcomatoid or rhabdoid differentiation provides a framework for prognostication and clinical decision-making in RCC. A high ISUP grade (grades 3–4), extensive necrosis, and dedifferentiated components identify patients at increased risk for recurrence and cancer-specific mortality, even in localized tumors at diagnosis. These features influence postoperative surveillance intensity and support consideration of adjuvant systemic therapy in selected high-risk patients [1,24].

In advanced and metastatic RCC, histologic features carry therapeutic implications. Sarcomatoid differentiation, despite poor prognosis, has shown improved response to immune checkpoint inhibitor–based regimens, now the preferred first-line options. Current clinical guidelines advocate for intensive follow-up and tailored systemic therapy for patients with high-grade or aggressive tumors [19].

Histologic subtype, ISUP grade, tumor necrosis, and dedifferentiation patterns are key determinants of RCC biological behavior. However, these factors are established only after surgical resection, highlighting the need for reliable, non-invasive imaging biomarkers to predict tumor aggressiveness before treatment. Advanced imaging techniques and radiomics show promise in this area.

3. Computed Tomography in the Evaluation of Renal Cell Carcinoma

3.1. Overview and Technical Role on CT in RCC

CT is the primary imaging modality for diagnosis, characterization, and staging of RCC. Contrast-enhanced multiphase CT is recommended for evaluating renal masses detected on ultrasound or other studies, with sensitivity of 88% and specificity of 75% for RCC detection and staging [3,25].

Standard renal mass protocols include an unenhanced phase followed by corticomedullary, nephrographic and excretory phases. This approach allows assessment of tumor size, location and enhancement characteristics, as well as detection of calcifications, internal heterogeneity, and hemorrhage. CT enables accurate evaluation of local tumor extension, renal sinus fat invasion, collecting system involvement, venous invasion, regional lymphadenopathy, and distant metastases, essential for TNM staging [26].

Triple-phase CT of the chest, abdomen, and pelvis is the standard imaging strategy for RCC staging, with accuracy of up to 91% for local staging [17]. CT plays a critical role in surgical planning, particularly for nephron-sparing procedures, by providing information on tumor anatomy, proximity to the collecting system, and renal vasculature [17,27].

Despite these advantages, conventional CT has limitations. It cannot reliably differentiate benign from malignant solid renal masses (Table 2), and substantial overlap exists in imaging appearances among RCC subtypes and benign lesions, such as oncocytoma or lipid-poor angiomyolipoma [17]. Emerging techniques, including DECT and multiparametric assessment strategies, are being investigated to enhance biologic characterization; however, standard contrast-enhanced CT remains the cornerstone of RCC imaging in clinical practice [9].

Table 2. CT imaging features associated with non-aggressive and aggressive renal tumors. .

 doi:10.20944/preprints202605.0012.v1

CT Imaging Feature	Non-Aggressive Renal Tumors	Aggressive Renal Tumors	Clinical/Pathological Correlation
Tumor Size	Small to moderate	Often large	Size correlates imperfectly with grade but reflects growth kinetics
Tumor Margins	Well-circumscribed	Ill-defined, infiltrative	Associated with capsular and perinephric invasion
Tumor Contour	Smooth or mildly lobulated	Deep lobulation, "saw-tooth" appearance	Linked to renal capsule invasion and poor prognosis
Internal Architecture	Homogeneous	Markedly heterogeneous	Reflects necrosis, hemorrhage and dedifferentiation
Enhancement pattern	Gradual or progressive enhancement	Early heterogeneous enhancement	Hypervascular components common in high-grade ccRCC
PTN	Absent or minimal	Enlarged/multiple peritumoral vessels	Correlates with higher Fuhrman/ISUP grade, advanced pT stage, ↓OS in ccRCC; may alter surgical planning
Mean Unenhanced Attenuation (HU)	Lower	Higher	Higher baseline HU linked to cellularity and reduced microscopic fat in aggressive RCC
Enhancement Difference (ΔHU)	Higher ΔHU, especially in nephrographic phase	Lower ΔHU	Lower enhancement predicts higher grade/recurrence; higher ΔHU associates with less aggressive biology
TCR	Higher	Lower	Normalizes to parenchyma; lower ratios in high-grade/aggressive RCC
DAR = cortex – tumor (HU)	Higher	Lower	Reduced cortex–tumor contrast in aggressive lesions
Degree of Enhancement	Low to moderate	Variable, often intense and irregular	Overlap exists among subtypes
Tumor Necrosis	Absent	Common	Independent adverse prognostic factor
Calcifications	Rare	May be present	Suggest malignancy and advanced disease
Venous Invasion	Absent	Renal vein or IVC tumor thrombus	Defines advanced stage and surgical complexity
Collecting System Involvement	Absent	May be present	Associated with high stage and poor outcome

 doi:10.20944/preprints202605.0012.v1

Perinephric Fat Invasion	Absent	Common	TNM upstaging
Regional Lymphadenopathy	Absent	More frequent	Advanced disease

ccRCC – clear cell Renal Cell Carcinoma; DAR – Difference Attenuation Ratio; HU – *Hounsfield Units;* ISUP – International Society of Urological Pathology; OS – Overall Survival; PTN – Peritumoral Neovascularity; pT – pathological Tumor staging; TCR – Tumor-to-cortex ratio.

3.2. Morphological CT Features Associated with Non-Aggressive Renal Tumors

CT features commonly associated with indolent or less aggressive renal tumors include homogeneous internal architecture, well-circumscribed margins, and gradual enhancement on multiphasic CT. These characteristics are frequent in papillary RCC, chromophobe RCC, and benign renal tumors. Papillary RCC typically appears as a hypovascular, homogeneous solid mass with low-level enhancement relative to adjacent renal parenchyma. Chromophobe RCC and oncocytoma often demonstrate moderate, relatively uniform enhancement and a well-defined interface with surrounding renal tissue. Oncocytomas may exhibit a central stellate scar (Figure 7), though this feature lacks specificity to differentiate them from malignant tumors [28–30].

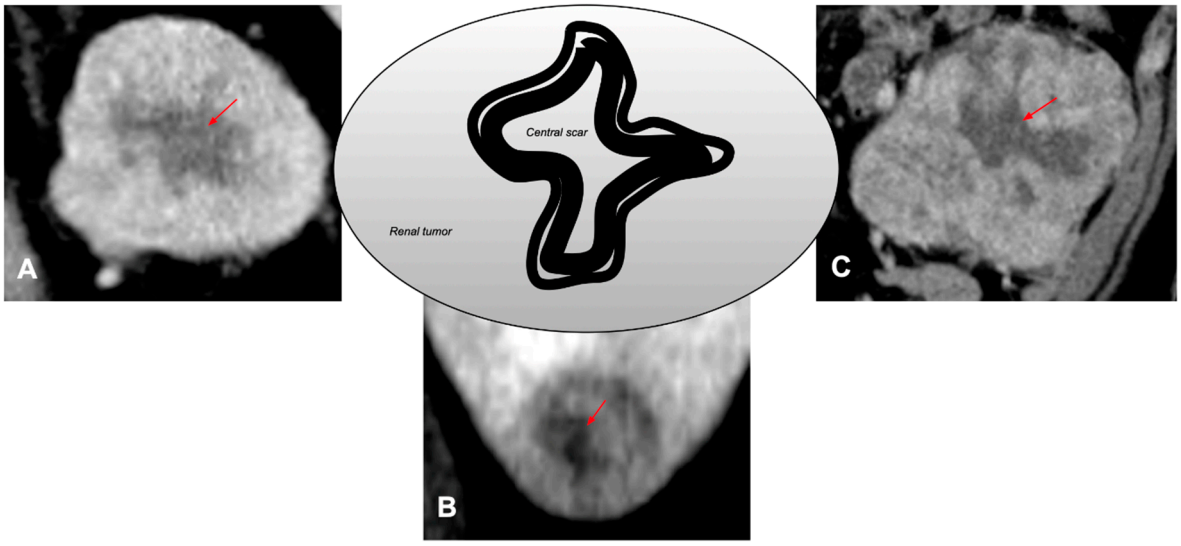

Figure 7. Examples of the "central scar" (red arrows) appearance on CT in an oncocytoma (A), Chromophobe renal cell carcinoma (B) and Clear Cell Renal Cell Carcinoma (C).

The absence of infiltrative margins, tumor necrosis, irregular enhancement, and vascular invasion supports a non-aggressive imaging phenotype. Progressive enhancement, versus early arterial hyperenhancement, has been associated with benignity, although sensitivity and specificity remain limited, as it occurs in papillary RCC. Macroscopic fat within a renal mass is diagnostic for classic angiomyolipoma, a benign lesion, whereas lipid-poor variants require careful evaluation of density and enhancement patterns [28,29,31].

Overlap exists between low-grade malignancies and benign renal tumors, and multiphase contrast-enhanced CT, while essential for characterization, may require adjunctive imaging or percutaneous biopsy for indeterminate lesions, as recommended by current American College of Radiology guidelines [8].

3.3. Morphological CT Features Associated with Aggressive Renal Tumors

Aggressive renal tumors often demonstrate distinctive but non-exclusive CT features reflecting advanced local invasion and unfavorable biology. These include ill-defined or infiltrative margins,

 doi:10.20944/preprints202605.0012.v1

irregular or deep lobulated contours, and the so-called "saw-tooth" sign (Figure 8), which associates with renal capsule invasion. Large tumor size and heterogeneous architecture are common findings. Heterogeneous enhancement with intermixed hypervascular soft-tissue components and non-enhancing necrotic or cystic areas is a hallmark of aggressive ccRCC. Tumor necrosis occurs more prevalently in high-grade RCC and correlates strongly with poor prognosis. Additional findings suggesting aggressive behavior include intralesional calcifications, collecting system involvement, and regional lymphadenopathy [3,29,31–34].

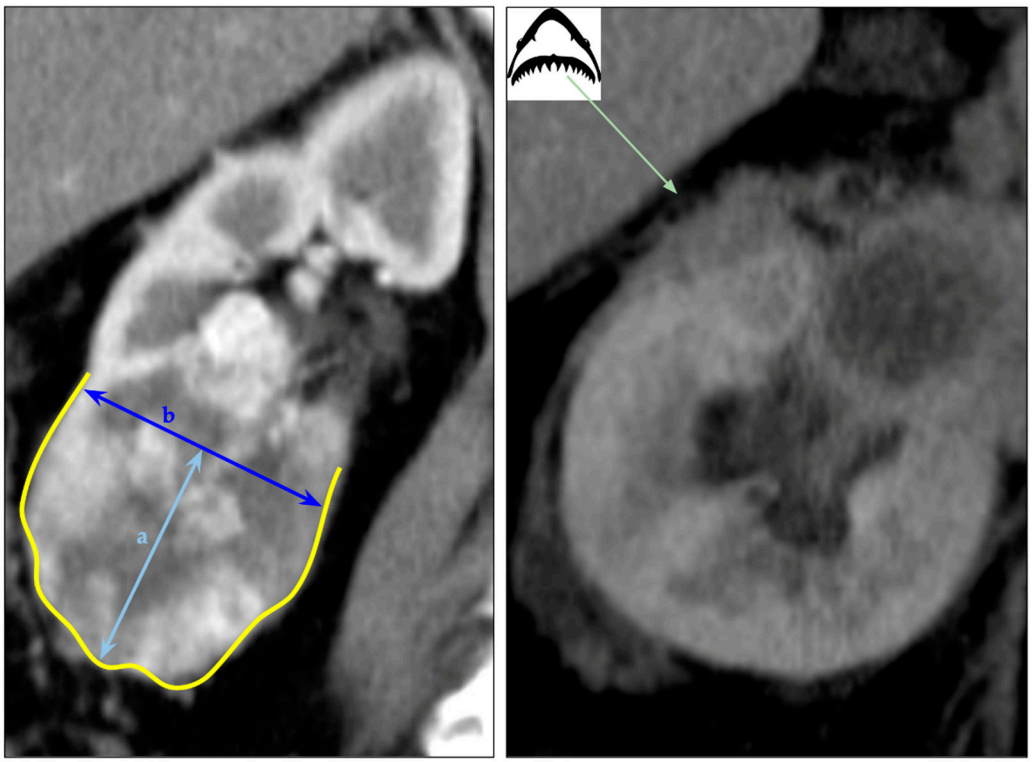

Figure 8. Left. The arc–chord distance (a) represents the maximal outward protrusion of the lobule, while the chord length (b) is the straight line connecting the two points at its base. The lobulated sign is classified as deep lobulation when the ratio of the arc-chord distance to the chord length is ≥0.4. Right. Sharp, irregular, and acute margin projections at the tumor–renal parenchyma interface representing the saw-tooth sign. .

Peritumoral neovascularity (Figure 9) is a significant biomarker of aggressive tumor biology. Enlarged or multiple vessels at the tumor–parenchymal interface on corticomedullary or nephrographic phase CT correlates with higher ISUP grade, advanced pathological stage and worse survival, even in small (T1a) tumors [35–37]. Quantitative scoring systems show that higher neovascularity scores are associated with pT2–pT3 disease and occur more frequently in ccRCC than other subtypes [38]. This feature reflects increased angiogenesis, a hallmark of aggressive behavior, and should guide surgical planning and follow-up strategies [34,39].

 doi:10.20944/preprints202605.0012.v1

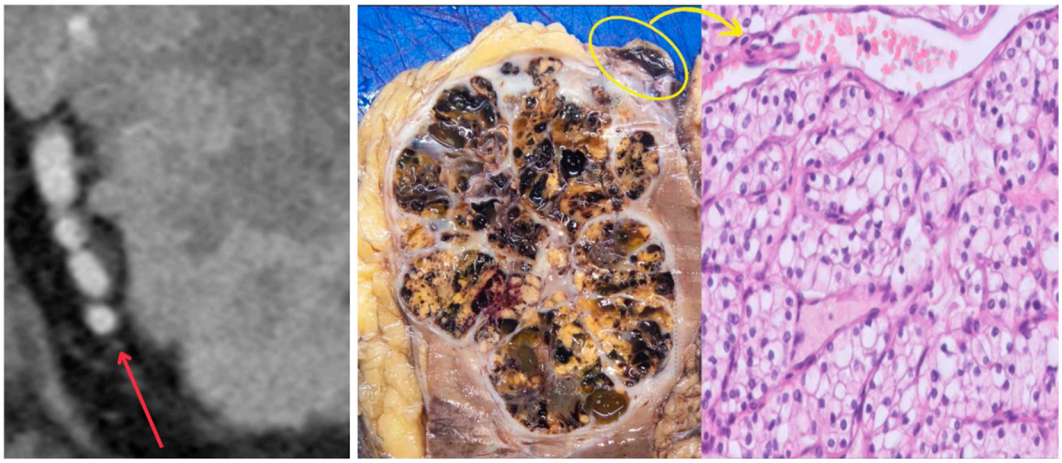

Figure 9. Prominent peritumoral vessels (red arrow). Histologically, they lack smooth muscle cells in their walls and may contain some fibrous connective tissue (yellow oval and arrow). .

CT is valuable for identifying venous invasion, including tumor thrombus extending into the renal vein or inferior vena cava, and direct extension into perinephric fat or adjacent structures (Figure 10). These features are critical for staging, surgical planning, and prognostication, as renal vein invasion, especially when involving the main renal vein or the vascular wall, independently associated with worse recurrence-free and cancer-specific survival. When renal vein invasion occurs with perinephric fat invasion, these tumors exhibit the poorest prognosis, with increased risk of disease progression and cancer-specific mortality [40,41].

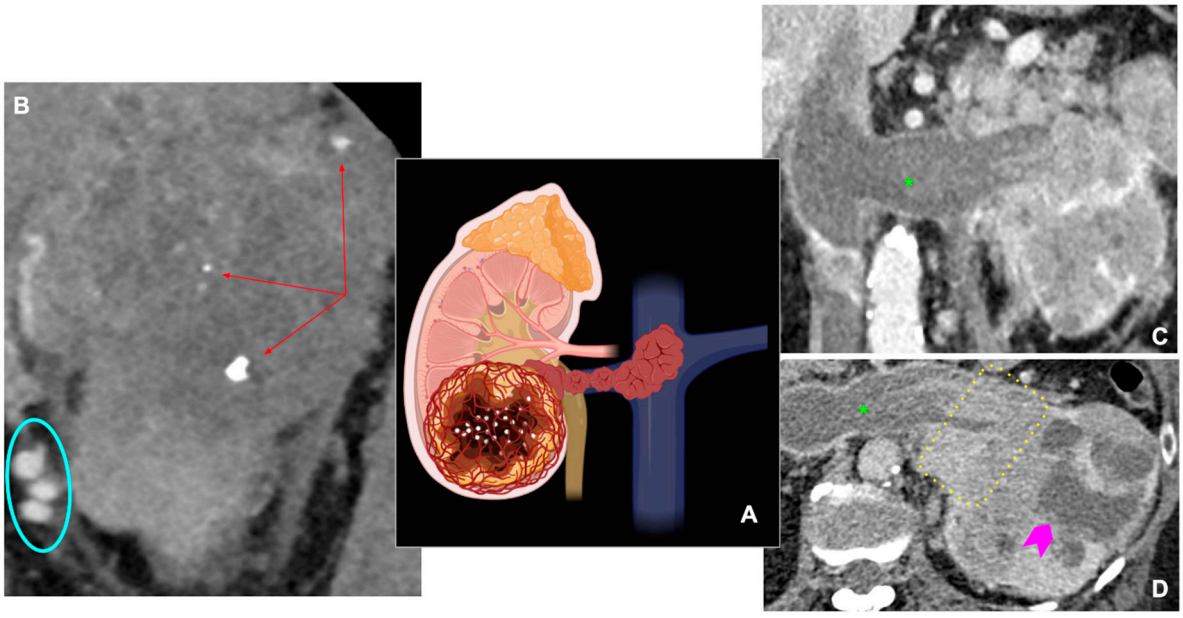

Figure 10. A. Central figure representing different morphological CT features associated with aggressive renal tumors. *Image created with BioRender*. B. Prominent peritumoral vessels (blue oval) and calcifications (red arrows) in a large heterogeneous renal mass. C, D. Ill-defined, infiltrating renal mass showing necrotic areas (pink arrowhead), venous tumoral thrombosis (*) and renal sinus infiltration (yellow rectangle). .

3.4. Dynamic CT Features

Dynamic CT parameters provide valuable quantitative biomarkers for characterizing renal tumors and estimating biological aggressiveness. These metrics are extracted from multiphasic CT

 doi:10.20944/preprints202605.0012.v1

acquisitions and include mean attenuation (N), attenuation difference (AD), tumor-to-cortex ratio (TCR), difference attenuation ratio (DAR), and volumetric heterogeneity measures.

Mean attenuation reflects tumor density on unenhanced CT (Figure 11). Aggressive RCCs, particularly high-grade ccRCC, show higher unenhanced attenuation values, due to increased cellularity and reduced microscopic fat content. Benign and indolent tumors often demonstrate lower baseline attenuation [42].

Attenuation difference (ΔHU), calculated as the change in Hounsfield units between pre-contrast and post-contrast phases, serves as a surrogate for tumor vascularity and enhancement (Figure 12). Higher ΔHU values, especially in the nephrographic phase, are associated with less aggressive biology and improved disease-free survival, whereas lower enhancement correlates with higher grade and increased recurrence risk [43].

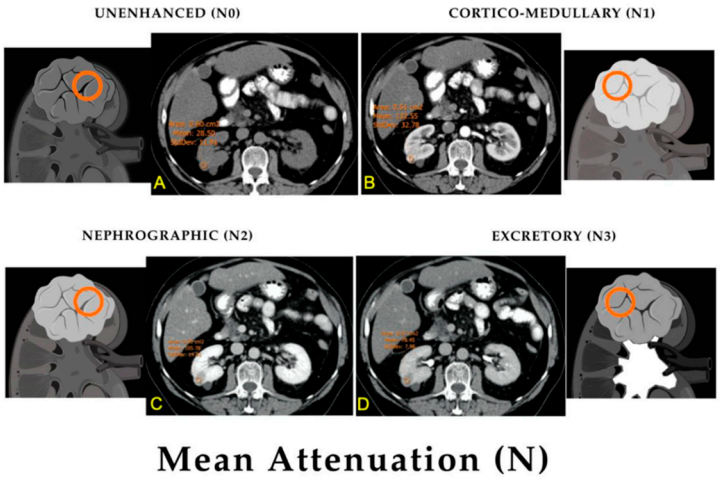

Figure 11. Mean Attenuation (N). *Images created with BioRender.*

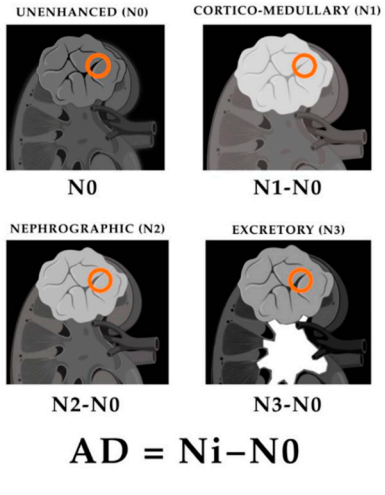

Figure 12. Attenuation Difference (AD). *Images created with BioRender.*

TCR (Figure 13) and DAR (Figure 14) normalize tumor enhancement to the adjacent renal parenchyma. Lower ratios and differences characterize aggressive RCC, while benign and indolent tumors exhibit higher ratios, reflecting more avid enhancement and preserved vascularity [42,44,45].

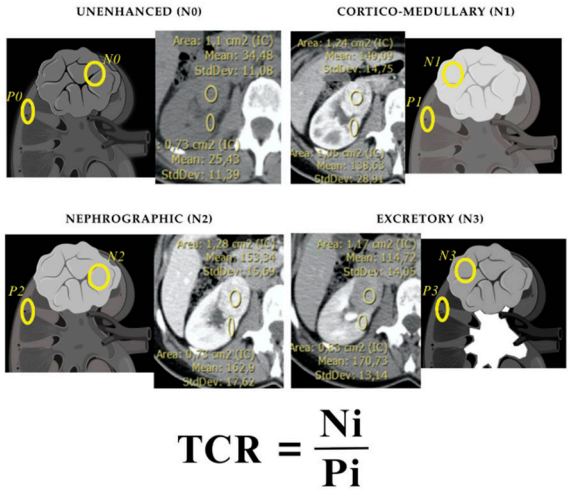

Figure 13. Tumor-to-Cortex ratio (TCR). *Images created with BioRender.*

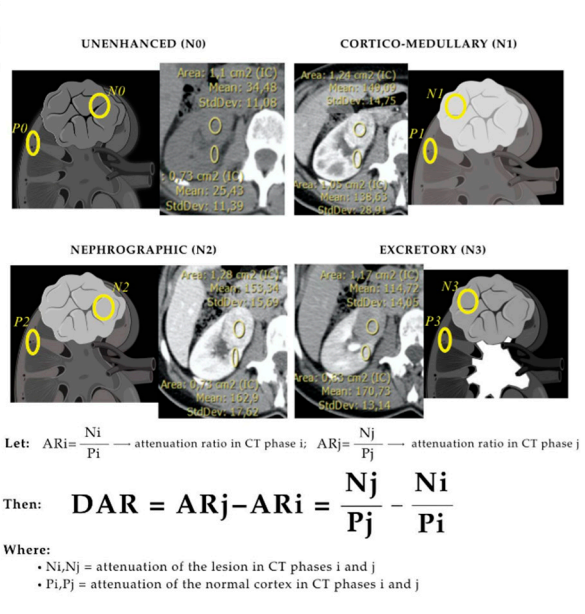

Figure 14. Difference in Attenuation Ratio (DAR). *Images created with BioRender.*

 doi:10.20944/preprints202605.0012.v1

Volumetric histogram analysis refines this assessment. Increased entropy and standard deviation within tumor volume indicate greater heterogeneity, a hallmark of aggressive ccRCC, whereas benign lesions display more homogeneous enhancement profiles [46].

3.5. Summary

Dynamic CT metrics complement qualitative imaging signs and provide a framework for preoperative risk stratification. Their integration into clinical practice offers potential to improve prediction of histologic grade and tumor behavior beyond visual interpretation.

Current guidelines emphasize multiphase contrast-enhanced CT in characterizing and staging renal masses, as aggressive imaging features influence management. However, even experienced radiologic assessment cannot fully capture tumor biology or predict histologic grade accurately, underscoring the need for quantitative imaging approaches to extract biological information from CT datasets.

4. CT and ISUP Grade: Radiological and Pathological Correlation

Accurate preoperative assessment of tumor grade remains a critical challenge in the management of RCC. Several studies have evaluated the diagnostic performance of CT imaging features alone, excluding radiomics, for predicting ISUP grade, reporting moderate accuracy with area under the curve (AUC) values from 0.75 to 0.85, sensitivity between 58% and 71%, and specificity from 79% to 90% [47,48]. These figures underscore the potential utility of CT-based assessment, while highlighting its limitations compared to histology.

4.1. Diagnostic Performance and Key Imaging Features

CT features most associated with ISUP grade include tumor size, attenuation values, enhancement patterns, and normalized iodine concentration (particularly in dual-energy CT). A multivariable model incorporating transverse diameter, unenhanced attenuation, and normalized iodine concentration achieved an AUC of 0.85, sensitivity of 70%, specificity of 90%, and overall accuracy of 82% for distinguishing low-grade from high-grade ccRCC [49]. Interobserver agreement for CT-based algorithms is generally good, with weighted kappa values around 0.71 for features such as mass-to-cortex attenuation ratio and heterogeneity score. Performance declines in small renal masses and in certain CT phases, such as the nephrographic phase, where feature discrimination is less pronounced [48].

4.2. Limitations and the Need for Quantitative Imaging

Despite its value, CT-based grading remains limited by moderate sensitivity, interobserver variability, and qualitative visual assessment. These limitations underscore the need for advanced imaging approaches capable of extracting deeper biologic information from routinely acquired CT datasets.

Radiomics shifts from qualitative interpretation to high-dimensional quantitative analysis. By extracting hundreds of features related to intensity, shape, and texture, radiomics enables robust modeling of tumor heterogeneity and microarchitecture, which correlate strongly with histologic grade. Recent studies demonstrate that combined models integrating radiomic features with clinical and imaging data outperform CT visual assessment, achieving AUC values exceeding 0.90 for ISUP grade prediction [47,50]. These findings highlight the promise of radiomics as a complementary tool for non-invasive prognostication and personalized management in patients with RCC.

5. Radiomics in Renal Cell Carcinoma

5.1. Radiomics Concept and Workflow

 doi:10.20944/preprints202605.0012.v1

Radiomics refers to the high-throughput extraction of quantitative features from medical images to convert imaging into mineable data for precision oncology [51,52]. Unlike visual interpretation, which is qualitative and observer-dependent, radiomics enables objective quantification of tumor phenotypes by analyzing patterns of intensity, shape, texture, and heterogeneity within a region (ROI) or volumne (VOI) of interest [53].

A standard radiomics pipeline includes (Figure 15): (1) standardized image acquisition; (2) tumor segmentation; (3) extraction of handcrafted features, including first-order, shape-based, and texture-based metrics; (4) feature selection to remove redundancy; and (5) development and validation of predictive models [52–55] .

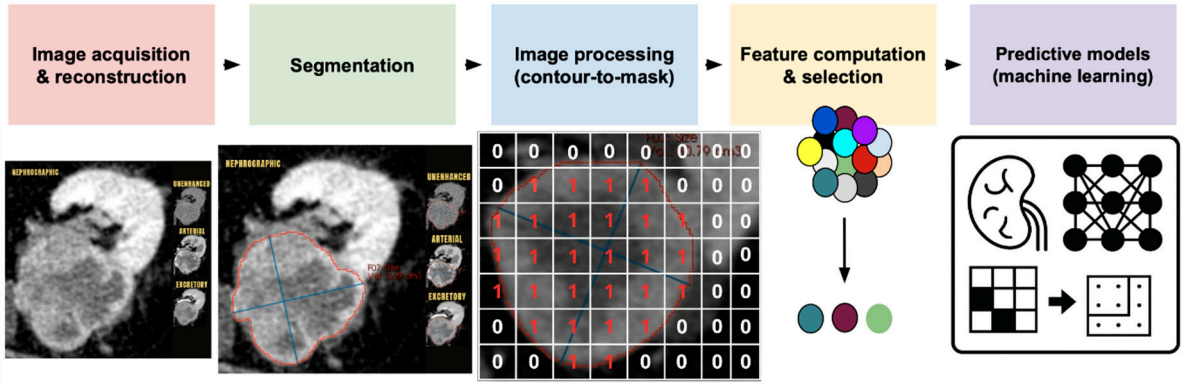

Figure 15. Radiomics Workflow. .

Radiomic features fall into four categories. First-order features from voxel intensity histograms describe properties like mean, median, variance, skewness, kurtosis, and entropy. Shape-based features quantify geometric properties including volume, surface area, sphericity, and compactness. Second-order (texture) features, computed from matrices such as the gray-level co-occurrence matrix (GLCM), gray-level run-length matrix (GLRLM), and gray-level size-zone matrix (GLSZM), characterize spatial relationships and patterns in voxel intensities, key markers of intratumoral heterogeneity. Higher-order features from filtered images (e.g., wavelet or Laplacian of Gaussian transforms) enable detection of multi-scale textural characteristics [56,57] (Table 3).

Features are selected based on reproducibility and relevance for building predictive models for diagnosis, prognosis, and treatment response. Dimensionality reduction and cross-validation help avoid overfitting and ensure generalizability [58].

Table 3. Mean Radiomics Features: Classification, Definition, and Clinical Interpretation. .

Feature Category	Feature Name	Definition	Clinical Interpretation
First-order (Intensity)	Mean Intensity	Average voxel value in ROI	Overall signal level; may reflect tissue density
	Entropy	Measure of randomness in voxel values	Heterogeneity; higher values suggest more complex tissue
	Skewness	Asymmetry of intensity distribution	Indicates deviation from normal tissue appearance
	Kurtosis	Peakedness of intensity distribution	High values may indicate abnormal tissue composition
Shape-based	Volume	Total size of the segmented region	Tumor burden; used for staging and response assessment
	Surface Area	Area of the ROI boundary	Tumor growth pattern; irregularity may suggest invasion

 doi:10.20944/preprints202605.0012.v1

	Sphericity	Degree to which shape approximates a sphere	Lower values suggest irregular or infiltrative tumors
Second-order (Texture-GLCM)	Contrast	Difference between neighboring voxel intensities	High values indicate marked heterogeneity
	Homogeneity	Uniformity of voxel pairs	High values suggest uniform tissue; low = heterogeneity
	Correlation	Linear dependency of gray levels	May reflect organized tissue structure
Second-order (Texture-GLRLM)	Short Run Emphasis	Frequency of short consecutive runs of similar intensity	High values = fine texture; low = coarse texture
	Zone Size Variance	Variability in size of homogeneous zones	High values = heterogeneous tissue architecture
Third-order	Wavelet Energy	Energy in specific frequency bands after wavelet transform	May capture subtle patterns

GLCM – gray-level co-occurrence matrix; GLRLM – gray-level run-length matrix; ROI – Region of Interest.

These features are extracted from ROIs or VOIs and interpreted for tumor biology, heterogeneity, and morphology. Standardization efforts, such as the Image Biomarker Standardization Initiative, have enabled reproducible feature definitions for clinical and research use [59].

Radiomics has proved valuable in oncology, with applications in lung, breast, prostate, hepatobiliary and abdominopelvic malignancies. Radiomic signatures improve diagnostic accuracy, risk stratification, and treatment response prediction, often surpassing conventional criteria [60–62].

5.2. Radiomics for Histologic Subtype Classification in RCC

One of the earliest clinical applications of radiomics in renal imaging was differentiating RCC subtypes and benign renal masses. Few studies have shown that handcrafted radiomic features from contrast-enhanced CT provide value for differentiating clear cell, papillary and chromophobe RCC, as well as RCC from oncocytoma [63–66] (Table 4).

Texture-based features, derived from gray-level co-occurrence and run-length matrices, including entropy, contrast and heterogeneity metrics, emerge as key discriminators, reflecting differences in tumor microarchitecture and heterogeneity [64,65,67–69]. Clear cell RCC exhibits greater textural variability than papillary RCC, which often shows lower enhancement and more homogeneous architecture [63,64]. For benign lesions, although oncocytoma remains difficult to characterize, lipid-poor angiomyolipoma is often recognized with higher accuracy [63].

Combined radiomics models integrating texture, shape and intensity features have demonstrated good diagnostic performance for differentiating RCC subtypes, with AUC values ranging from 0.80 in multicenter studies to above 0.90 in unicentric analyses [65,69,70]. These models outperform qualitative visual assessment and alone CT metrics, such as size or enhancement alone.

Table 4. Radiomics Findings by Histologic Subtype in Renal Tumors (CT-Based Radiomics) .

Histologic Subtype	Biological/Imaging Characteristics	Relevant Radiomics Features Reported	Performance	Remarks and Limitations

 doi:10.20944/preprints202605.0012.v1

	Captured by Radiomics			
ccRCC	Marked intratumoral heterogeneity; hypervascularity; complex microarchitecture	Texture features (GLCM entropy, contrast, homogeneity); GLRLM run-entropy; wavelet-derived features; combination with shape and intensity metrics	~0.75 in multiclass models with external validation; up to 0.82–0.96 in selected binary or single-center studies	Performance decreases in multiclass settings and with external validation; sensitive to acquisition and reconstruction variability
pRCC	Hypovascular tumors with relatively homogeneous architecture compared with ccRCC	First-order histogram features; GLCM homogeneity/energy; low entropy metrics	Comparable to ccRCC in binary models (often within 0.80–0.90); lower accuracy in multiclass classification	Limited robustness due to frequent overlap with oncocytoma and chromophobe RCC
chRCC	Relatively homogeneous cellular structure; subtle differences from oncocytoma	GLCM contrast and entropy; GLSZM zone variance; shape features (flatness, surface-to-volume ratio)	RO vs chRCC: high performance (AUC ~0.94–0.99) in dedicated binary models, including external validation	Excellent performance in targeted binary tasks; generalizability depends on standardized protocols
RO	Benign tumor with overlapping imaging phenotype; low-grade heterogeneity	Texture features indicating low heterogeneity; combination with morphological and enhancement features	Multiclass classification: limited performance (AUC ~0.57–0.69); RO vs RCC (meta-analysis): sensitivity ~0.82, specificity ~0.81	Most challenging subtype; substantial overlap with chRCC; performance improves with combined clinical or nomogram-based models
LP-AML	Distinct textural and intensity patterns reflecting mesenchymal composition	First-order intensity features; texture metrics; shape descriptors	High accuracy (AUC ~0.90–0.94)	Generally easier to identify than oncocytoma in radiomics-based models

*Reported AUC ranges depend on study design, cohort size, imaging phase, and presence of external validation. AUC – Area Under the Curve; ccRCC – clear cell Renal Cell Carcinoma; chRCC – chromophobe Renal Cell Carcinoma; LP-AML – Lipid Poor Angiomyolipoma; pRCC – papillary Renal Cell Carcinoma; RO – Renal Oncocytoma;.

In clinical practice, accurate subtype prediction using imaging alone remains challenging. Radiomics offers value by capturing microarchitectural differences and may guide individualized

 doi:10.20944/preprints202605.0012.v1

management strategies, particularly in small renal masses where biopsy is inconclusive or not feasible.

5.3. Radiomics for Predicting ISUP Grade and Tumor Aggressiveness

Recent validation studies and meta-analyses show radiomics-based models outperform traditional clinicopathological models in assessing tumor aggressiveness in patients with renal tumors, particularly ccRCC (Table 5). Radiomics models using CT or MRI features, especially texture features quantifying tumor heterogeneity, achieve higher diagnostic accuracy for preoperative grading and aggressiveness assessment. Meta-analyses report pooled AUC values of 0.84–0.88 for radiomics models, compared to lower AUCs for clinicopathological models [71,72]. Combined models integrating radiomics with clinical variables improve performance, with pooled AUCs up to 0.90 and higher sensitivity for detecting high-grade disease [72].

Radiomics features associated with intratumoral heterogeneity strongly correlated with aggressive histopathologic characteristics in RCC. High entropy, increased variance, and low homogeneity on CT or MRI reflect marked spatial heterogeneity within the tumor and indicate necrosis and high-grade histology. These features capture disordered tissue organization and heterogeneous cellular density, hallmarks of aggressive tumors [34]. Sarcomatoid differentiation has pronounced radiomic heterogeneity, with increased textural complexity indicated by elevated GLCM contrast, cluster shade, run-length non-uniformity, and irregular shape features [73,74]. These metrics reflect architectural distortion and loss of organized tumor structure, correlating with poor prognosis.

Microvascular invasion is best predicted by composite radiomics signatures integrating texture-based metrics with first-order intensity features. These signatures can capture imaging correlates of vascular infiltration not visible on conventional imaging [75,76].

Table 5. Radiomics Features Correlated with Aggressive Histological Factors in RCC. .

Radiomics Feature	Definition/ Type	Correlated Aggressive Histological Factor(s)	Interpretation
Entropy	Texture (GLCM)	Necrosis, Sarcomatoid differentiation	High heterogeneity; associated with necrosis and dedifferentiation
Cluster Shade	Texture (GLCM)	Sarcomatoid differentiation	Asymmetry in texture; linked to aggressive dedifferentiation
Contrast	Texture (GLCM)	Necrosis, Sarcomatoid differentiation	Intensity variation; higher in necrotic/aggressive tumors
Homogeneity	Texture (GLCM)	Necrosis	Lower values indicate more heterogeneity and necrosis
Corelation	Texture (GLCM)	Microvascular invasion, High grade	Linear dependency of gray levels; may reflect organized vs. disrupted tissue
Skewness	First-order (Intensity)	Necrosis, High grade	Asymmetric intensity distribution; deviation from normal tissue
Kurtosis	First-order (Intensity)	Necrosis, High grade	Peaked intensity distribution; abnormal tissue composition
Median Intensity	First-order (Intensity)	Necrosis, High grade	Lower median values associated with necrosis/high grade

 doi:10.20944/preprints202605.0012.v1

Variance	First-order (Intensity)	Necrosis, High grade	Higher variance reflects heterogeneity and aggressive features
Run-Length Non-Uniformity	Texture (GLRLM)	Sarcomatoid differentiation	Higher values indicate heterogeneous texture; linked to dedifferentiation
Gray-Level Non-Uniformity	Texture (GLRLM)	Microvascular invasion, High grade	Higher values mean heterogeneous tissue architecture
Zone Size Variance	Texture (GLSZM)	Microvascular invasion, Poor prognosis	Irregular shape; associated with vascular invasion and poor outcome
Flatness	Shape	Microvascular invasion, Poor prognosis	Irregular shape; associated with vascular invasion and poor outcome
Area Density	Shape	Microvascular invasion, Poor prognosis	Tumor compactness; lower density linked to aggressive features
Sphericity	Shape	Sarcomatoid differentiation, High grade	Lower values suggest irregular or infiltrative tumors
Wavelet Energy	Higher-order (Wavelet)	High grade, Necrosis, Recurrence	Captures subtle multi-scale heterogeneity; linked to aggressive phenotypes

GLCM – gray-level co-occurrence matrix; GLRLM – gray-level run-length matrix; GLSZM – Gray-Level Size Zone Matrix.

In summary, radiomics-based models provide more accurate assessment of tumor aggressiveness in renal tumors than traditional models, especially when combined with clinical data. However, their clinical integration requires further prospective validation and standardization to ensure reproducibility and generalizability across institutions.

5.4. Prognostic Radiomics: Recurrence, Survival and Treatment Response

Radiomics-based tumor heterogeneity scores, derived from clustering texture features, have been validated as predictors of recurrence and poor clinical outcome [76–78].

Texture features such as entropy, cluster shade, and GLCM metrics quantify tumor heterogeneity, associated with aggressive biology and recurrence risk [76,78]. Shape features and intensity features have been independently linked to survival [79,80]. Wavelet-transformed texture features enhance prognostic accuracy by multi-scale heterogeneity [81]. Radiomics signatures combining these features outperform conventional models in predicting recurrence and survival in RCC. Growing evidence confirms that radiomics signatures provide superior prognostic value for overall survival and recurrence risk (C-statistics, 0.84–0.92) compared to established models like TNM, SSIGN, and Leibovich scores (C-statistics, 0.64–0.78) [71,76,78].

Decision curve analyses show radiomics-based models may offer clinical benefits for guiding adjuvant therapy and surveillance decisions in high-risk populations when combined with clinical data [76].

 doi:10.20944/preprints202605.0012.v1

Radiomic signatures show promise in predicting immune checkpoint inhibitors' response in RCC. Higher tumor intensity variance, maximum intensity, and non-uniformity on baseline CT correlate with progression and poor immunotherapy response [82]. Radiomic features like energy, run length non-uniformity, busyness, and gray-level non-uniformity can identify minimal residual disease after immune checkpoint blockade (AUC >0.84) [83]. Finally, radiomics-derived heterogeneity correlates with immune phenotypes, with higher scores indicating increased tumor-infiltrating CD8+ cells and better anti-PD-1/PD-L1 therapy response [84].

Therefore, radiomics can non-invasively characterize the tumor microenvironment and may help stratify patients for immunotherapy. However, while radiomics-based prediction of immunotherapy response shows promise, further validation and standardization are needed before clinical implementation [85,86].

5.5. Limitations and Challenges of Radiomics in RCC

Despite growing interest in radiomics for RCC, methodological and practical limitations hinder its clinical adoption.

First, significant heterogeneity in imaging acquisition protocols, segmentation strategies, feature extraction methods, and machine-learning workflows undermining reproducibility and generalizability across institutions. Most studies are retrospective and single-center, usually lacking standardized imaging protocols or external validation, leading to inconsistent performance and limited real-world applicability [86].

Second, the methodological quality of radiomics studies remains suboptimal. Radiomics Quality Scores (RQS) are low due to lack of prospective validation, harmonized pipelines, open-source code, data sharing, transparency, and verification [69,86].

Third, tumor segmentation causes much variability. Manual segmentation is susceptible to reader inconsistencies, while automated methods remain inadequately validated. Small differences in tumor delineation can alter extracted features and predictions. Few studies have addressed segmentation reproducibility [87].

Fourth, high-dimensional feature sets from small datasets can cause overfitting. Models may develop well but not generalize. Cross-validation alone cannot guarantee robustness [69,86,88]. Fifth, there is no consensus on optimal feature selection, harmonization, or validation strategies. Many analyses rely on internal cross-validation, with few using external validation cohorts [87,88].

Finally, integrating radiomics into clinical workflows remains challenging. Models must be interpretable, reliable, and seamlessly integrated into radiology and multidisciplinary decision-making pathways. Clinical translation is delayed by lack of trials and guidelines [50,86]. Multicenter collaboration, standardized pipelines, open science, and rigorous prospective validation are needed to overcome these limitations.

6. Future Steps for Characterization of Renal Cell Carcinoma and Clinical Usage

Radiomics and AI-based imaging tools show potential for improving non-invasive characterization of RCC, particularly in assessing tumor heterogeneity, aggressiveness, and molecular features. Their ability to distinguish benign from malignant masses, predict grades, and estimate outcomes is promising. However, clinical translation is limited by methodological heterogeneity, lack of validation, and low RQS, reflecting reproducibility and standardization issues.

Progress in RCC characterization requires emphasis on standardization, reproducibility, and methodological rigor. Harmonization of imaging acquisition protocols across CT, multiparametric MRI, and DECT, with guidelines for feature extraction, preprocessing, and feature selection, will reduce inter-institutional variability. Open science practices will enable verification of radiomics signatures. The Image Biomarker Standardization Initiative (IBSI) supports radiomics definitions and workflows.

Clinical translation depends on prospective, multicenter trials validating radiomics models across diverse cohorts and imaging platforms. Integration of radiomics with clinical, pathological,

 doi:10.20944/preprints202605.0012.v1

and molecular biomarkers can enhance risk prediction, treatment selection, and surveillance. Emerging technologies like photon-counting CT, molecular imaging tracers, and advanced AI architectures may enable more accurate virtual biopsy and tumor biology assessment [9,89]. Advancements in imaging classification systems enhance diagnostic precision and support refined management algorithms. The future of radiomics in RCC depends on overcoming barriers through standardization, reproducibility, and validation. Multicenter collaboration, open science initiatives, harmonized workflows, and integration with clinical and molecular data are needed to develop reliable radiomics for personalized RCC care.

7. Conclusions

Multiphasic CT remains essential for characterizing RCC, yet conventional radiologic assessment alone cannot fully capture the biological heterogeneity, histologic grade, or aggressiveness. Radiomics provides a powerful, non-invasive quantitative approach that outperforms traditional imaging and clinical models in predicting tumor subtypes, grades, recurrence, survival, and immunotherapy response. Progress will depend on standardized acquisition protocols, multicenter validation, and integration of radiomics with clinical and molecular data to enable reliable, personalized RCC management.

References

1. Young, M.; Jackson-Spence, F.; Beltran, L.; Day, E.; Suarez, C.; Bex, A.; Powles, T.; Szabados, B. Renal Cell Carcinoma. *The Lancet* **2024**, *404*, 476–491, doi:10.1016/S0140-6736(24)00917-6.
2. Larcher, A.; Campi, R.; Bex, A.; Bray, F.; Bukavina, L.; Jonasch, E.; Jemal, A.; Marston Linehan, W.; Marandino, L.; Mir, M.C.; et al. Epidemiology of Renal Cancer: Incidence, Mortality, Survival, Genetic Predisposition, and Risk Factors. *Eur. Urol.* **2025**, *88*, 341–358, doi:10.1016/j.eururo.2025.06.005.
3. Rose, T.L.; Kim, W.Y. Renal Cell Carcinoma: A Review. *JAMA* **2024**, *332*, 1001, doi:10.1001/jama.2024.12848.
4. Sepp, T.; Poyhonen, A.; Uusküla, A.; Kotsar, A.; Veitonmäki, T.; Tammela, T.L.J.; Baburin, A.; Murtola, T.J. Renal Cancer Survival in Clear Cell Renal Cancer Compared to Other Types of Tumor Histology: A Population-Based Cohort Study. *PLOS One* **2025**, *20*, e0329000, doi:10.1371/journal.pone.0329000.
5. Hong, B.; Hou, H.; Chen, L.; Li, Z.; Zhang, Z.; Zhao, Q.; Du, X.; Li, Y.; Ye, X.; Xu, W.; et al. The Clinicopathological Features and Prognosis in Patients With Papillary Renal Cell Carcinoma: A Multicenter Retrospective Study in Chinese Population. *Front. Oncol.* **2021**, *11*, 753690, doi:10.3389/fonc.2021.753690.
6. Campbell, S.C.; Clark, P.E.; Chang, S.S.; Karam, J.A.; Souter, L.; Uzzo, R.G. Renal Mass and Localized Renal Cancer: Evaluation, Management, and Follow-Up: AUA Guideline: Part I. *J. Urol.* **2021**, *206*, 199–208, doi:10.1097/JU.0000000000001911.
7. Campbell, S.C.; Uzzo, R.G.; Karam, J.A.; Chang, S.S.; Clark, P.E.; Souter, L. Renal Mass and Localized Renal Cancer: Evaluation, Management, and Follow-up: AUA Guideline: Part II. *J. Urol.* **2021**, *206*, 209–218, doi:10.1097/JU.0000000000001912.
8. Wang, Z.J.; Nikolaidis, P.; Khatri, G.; Dogra, V.S.; Ganeshan, D.; Goldfarb, S.; Gore, J.L.; Gupta, R.T.; Hartman, R.P.; Heilbrun, M.E.; et al. ACR Appropriateness Criteria® Indeterminate Renal Mass. *J. Am. Coll. Radiol.* **2020**, *17*, S415–S428, doi:10.1016/j.jacr.2020.09.010.
9. Bellin, M.-F.; Valente, C.; Bekdache, O.; Maxwell, F.; Balasa, C.; Savignac, A.; Meyrignac, O. Update on Renal Cell Carcinoma Diagnosis with Novel Imaging Approaches. *Cancers* **2024**, *16*, 1926, doi:10.3390/cancers16101926.
10. Bellini, D.; Panvini, N.; Laghi, A.; Marin, D.; Patel, B.N.; Wang, C.L.; Carbone, I.; Mileto, A. Systematic Review and Meta-Analysis Investigating the Diagnostic Yield of Dual-Energy CT for Renal Mass Assessment. *Am. J. Roentgenol.* **2019**, *212*, 1044–1053, doi:10.2214/AJR.18.20625.
11. Laothamatas, I.; Al Mubarak, H.; Reddy, A.; Wax, R.; Badani, K.; Taouli, B.; Bane, O.; Lewis, S. Multiparametric MRI of Solid Renal Masses: Principles and Applications of Advanced Quantitative and Functional Methods for Tumor Diagnosis and Characterization. *J. Magn. Reson. Imaging* **2023**, *58*, 342–359, doi:10.1002/jmri.28718.

 doi:10.20944/preprints202605.0012.v1

12. Tsili, A.C.; Moulopoulos, L.-A.; Varakarakis, I.M.; Argyropoulou, M.I. Cross-Sectional Imaging Assessment of Renal Masses with Emphasis on MRI. *Acta Radiol.* **2022**, *63*, 1570–1587, doi:10.1177/02841851211052999.
13. Cornelis, F.; Tricaud, E.; Lasserre, A.S.; Petitpierre, F.; Bernhard, J.C.; Le Bras, Y.; Yacoub, M.; Bouzgarrou, M.; Ravaud, A.; Grenier, N. Multiparametric Magnetic Resonance Imaging for the Differentiation of Low and High Grade Clear Cell Renal Carcinoma. *Eur. Radiol.* **2015**, *25*, 24–31, doi:10.1007/s00330-014-3380-x.
14. Cui, E.; Li, Z.; Ma, C.; Li, Q.; Lei, Y.; Lan, Y.; Yu, J.; Zhou, Z.; Li, R.; Long, W.; et al. Predicting the ISUP Grade of Clear Cell Renal Cell Carcinoma with Multiparametric MR and Multiphase CT Radiomics. *Eur. Radiol.* **2020**, *30*, 2912–2921, doi:10.1007/s00330-019-06601-1.
15. Serter, A.; Onur, M.R.; Coban, G.; Yildiz, P.; Armagan, A.; Kocakoc, E. The Role of Diffusion-Weighted MRI and Contrast-Enhanced MRI for Differentiation between Solid Renal Masses and Renal Cell Carcinoma Subtypes. *Abdom. Radiol.* **2021**, *46*, 1041–1052, doi:10.1007/s00261-020-02742-w.
16. Schieda, N.; Krishna, S.; Pedrosa, I.; Kaffenberger, S.D.; Davenport, M.S.; Silverman, S.G. Active Surveillance of Renal Masses: The Role of Radiology. *Radiology* **2022**, *302*, 11–24, doi:10.1148/radiol.2021204227.
17. Stewart, G.D.; Klatte, T.; Cosmai, L.; Bex, A.; Lamb, B.W.; Moch, H.; Sala, E.; Siva, S.; Porta, C.; Gallieni, M. The Multispeciality Approach to the Management of Localised Kidney Cancer. *The Lancet* **2022**, *400*, 523–534, doi:10.1016/S0140-6736(22)01059-5.
18. Cohen, H.T.; McGovern, F.J. Renal-Cell Carcinoma. *N. Engl. J. Med.* **2005**, 353, 2477–2490, doi:10.1056/NEJMra043172.
19. Trpkov, K.; Hes, O.; Williamson, S.R.; Adeniran, A.J.; Agaimy, A.; Alaghehbandan, R.; Amin, M.B.; Argani, P.; Chen, Y.-B.; Cheng, L.; et al. New Developments in Existing WHO Entities and Evolving Molecular Concepts: The Genitourinary Pathology Society (GUPS) Update on Renal Neoplasia. *Mod. Pathol.* **2021**, *34*, 1392–1424, doi:10.1038/s41379-021-00779-w.
20. Delahunt, B.; Eble, J.N.; Egevad, L.; Samaratunga, H. Grading of Renal Cell Carcinoma. *Histopathology* **2019**, *74*, 4–17, doi:10.1111/his.13735.
21. Li, Y.; Lih, T.-S.M.; Dhanasekaran, S.M.; Mannan, R.; Chen, L.; Cieslik, M.; Wu, Y.; Lu, R.J.-H.; Clark, D.J.; Kołodziejczak, I.; et al. Histopathologic and Proteogenomic Heterogeneity Reveals Features of Clear Cell Renal Cell Carcinoma Aggressiveness. *Cancer Cell* **2023**, *41*, 139-163.e17, doi:10.1016/j.ccell.2022.12.001.
22. Kryvenko, O.N. Tumor Necrosis Adds Prognostically Significant Information to Grade in Clear Cell Renal Cell Carcinoma: A Study of 842 Consecutive Cases from a Single Institution. Khor LY, Dhakal HP, Jia X, Reynolds JP, McKenney JK, Rini BI, Magi-Galluzzi C, Przybycin CG.Am J Surg Pathol. September 2016;40(9):1224–1231. *Urol. Oncol. Semin. Orig. Investig.* **2017**, *35*, 454–455, doi:10.1016/j.urolonc.2017.03.023.
23. Delahunt, B.; Cheville, J.C.; Martignoni, G.; Humphrey, P.A.; Magi-Galluzzi, C.; McKenney, J.; Egevad, L.; Algaba, F.; Moch, H.; Grignon, D.J.; et al. The International Society of Urological Pathology (ISUP) Grading System for Renal Cell Carcinoma and Other Prognostic Parameters. *Am. J. Surg. Pathol.* **2013**, *37*, 1490–1504, doi:10.1097/PAS.0b013e318299f0fb.
24. Choi, J.; Bang, S.; Suh, J.; Choi, C.I.; Song, W.; Yuk, H.D.; Lee, C.H.; Kang, M.; Choo, S.H.; Kim, J.K.; et al. Survival Pattern of Metastatic Renal Cell Carcinoma Patients According to WHO/ISUP Grade: A Long-Term Multi-Institutional Study. *Sci. Rep.* **2024**, *14*, 4740, doi:10.1038/s41598-024-54052-6.
25. Vogel, C.; Ziegelmüller, B.; Ljungberg, B.; Bensalah, K.; Bex, A.; Canfield, S.; Giles, R.H.; Hora, M.; Kuczyk, M.A.; Merseburger, A.S.; et al. Imaging in Suspected Renal-Cell Carcinoma: Systematic Review. *Clin. Genitourin. Cancer* **2019**, *17*, e345–e355, doi:10.1016/j.clgc.2018.07.024.
26. Elkassem, A.A.; Allen, B.C.; Sharbidre, K.G.; Rais-Bahrami, S.; Smith, A.D. Update on the Role of Imaging in Clinical Staging and Restaging of Renal Cell Carcinoma Based on the AJCC 8th Edition, From the *AJR* Special Series on Cancer Staging. *Am. J. Roentgenol.* **2021**, *217*, 541–555, doi:10.2214/AJR.21.25493.
27. Sheth, S.; Scatarige, J.C.; Horton, K.M.; Corl, F.M.; Fishman, E.K. Current Concepts in the Diagnosis and Management of Renal Cell Carcinoma: Role of Multidetector CT and Three-Dimensional CT. *RadioGraphics* **2001**, *21*, S237–S254, doi:10.1148/radiographics.21.suppl_1.g01oc18s237.
28. Millet, I.; Doyon, F.C.; Hoa, D.; Thuret, R.; Merigeaud, S.; Serre, I.; Taourel, P. Characterization of Small Solid Renal Lesions: Can Benign and Malignant Tumors Be Differentiated With CT? *Am. J. Roentgenol.* **2011**, *197*, 887–896, doi:10.2214/AJR.10.6276.

 doi:10.20944/preprints202605.0012.v1

29. Mancini, M.E.; Albergo, A.; Moschetta, M.; Angelelli, M.; Scardapane, A.; Angelelli, G. Diagnostic Potential of Multidetector Computed Tomography for Characterizing Small Renal Masses. *Sci. World J.* **2015**, *2015*, 476750, doi:10.1155/2015/476750.
30. Krishna, S.; Murray, C.A.; McInnes, M.D.; Chatelain, R.; Siddaiah, M.; Al-Dandan, O.; Narayanasamy, S.; Schieda, N. CT Imaging of Solid Renal Masses: Pitfalls and Solutions. *Clin. Radiol.* **2017**, *72*, 708–721, doi:10.1016/j.crad.2017.05.003.
31. Zhang, J.; Lefkowitz, R.A.; Ishill, N.M.; Wang, L.; Moskowitz, C.S.; Russo, P.; Eisenberg, H.; Hricak, H. Solid Renal Cortical Tumors: Differentiation with CT. *Radiology* **2007**, *244*, 494–504, doi:10.1148/radiol.2442060927.
32. Nicolau, C.; Ivars, A.; Sebastia, C.; Bassaganyas, C.; Fresno, M.; Rodríguez, L.; Puig, J.; Comas-Cufí, M.; Paño, B. Computed Tomography of Neoplastic Infiltrating Renal Masses in Patients Without a Previous History of Cancer. *Cancers* **2025**, *17*, 2936, doi:10.3390/cancers17172936.
33. Zhang, Y.; Tian, H.; Zhang, S.; Zhang, Q.; Wu, X. Multislice Spiral Computed Tomography Signs of Invasion of the Renal Capsule by Renal Cell Carcinoma. *Medicine (Baltimore)* **2018**, *97*, e13075, doi:10.1097/MD.0000000000013075.
34. Krishna, S.; Kandasamy, M.; Bhayana, R.; Schieda, N. Imaging Biomarkers in Evaluation of Malignancy and Aggressiveness in Renal Masses. *Radiol. Clin. North Am.* **2025**, *63*, 873–888, doi:10.1016/j.rcl.2025.03.016.
35. Zhang, J.; Lefkowitz, R.A.; Wang, L.; Ishill, N.M.; Moskowitz, C.S.; Russo, P.; Hricak, H. Significance of Peritumoral Vascularity on CT in Evaluation of Renal Cortical Tumor: *J. Comput. Assist. Tomogr.* **2007**, *31*, 717–723, doi:10.1097/rct.0b013e318031521e.
36. Li, C.; Cen, D.; Liu, Z.; Liang, C. Presence of Intratumoral Calcifications and Vasculature Is Associated With Poor Overall Survival in Clear Cell Renal Cell Carcinoma. *J. Comput. Assist. Tomogr.* **2018**, *42*, 418–422, doi:10.1097/RCT.0000000000000704.
37. Ghiraldi, E.M.; Nguyen, J.; Buck, M.; Nair, H.; Israel, G.; Singh, D. Using Peritumor and Intratumor Vascularity on Preoperative Imaging to Predict Fuhrman Grade Histology of Renal Tumors. *J. Endourol.* **2022**, *36*, 1489–1494, doi:10.1089/end.2022.0069.
38. Fateri, C.; Peta, A.; Limfueco, L.; Bui, T.-L.; Kar, N.; Glavis-Bloom, J.; Roth, B.; Landman, J.; Houshyar, R. Novel Retroperitoneal Neovascularity Scoring System in Renal Cell Carcinoma Tumor Staging. *J. Endourol.* **2023**, *37*, 367–373, doi:10.1089/end.2022.0338.
39. Bauman, T.M.; Huang, W.; Lee, M.H.; Abel, E.J. Neovascularity as a Prognostic Marker in Renal Cell Carcinoma. *Hum. Pathol.* **2016**, *57*, 98–105, doi:10.1016/j.humpath.2016.07.005.
40. Lee, H.Y.; Lee, R.R.; Kim, Y.; Oh, J.-H.; Suh, J.; Jeong, C.-W.; Kwak, C.; Kang, M.; Seo, S.I.; Woo, H.-N.; et al. Distinct Prognostic and Molecular Profiles of Fat versus Vein Invasion in T3a Renal Cell Carcinoma. *Br. J. Cancer* **2025**, *133*, 1888–1895, doi:10.1038/s41416-025-03230-y.
41. Lai, G.-S.; Li, J.-R.; Wang, S.-S.; Chen, C.-S.; Yang, C.-K.; Hung, S.-C.; Cheng, C.-L.; Ou, Y.-C.; Chiu, K.-Y. Prognostic Evaluation of the Site of Invasion in Pathological Stage T3a Renal Cell Carcinoma. In Vivo **2021**, *35*, 1083–1089, doi:10.21873/invivo.12353.
42. Pickovsky, J.S.; Alo Nasiyabi, K.; Eldihimi, F.; Schieda, N. Utility of Multiparametric Renal CT for Differentiation of Low-Grade from High-Grade cT1a Clear Cell Renal Cell Carcinoma. *Br. J. Radiol.* **2023**, *96*, 20221087, doi:10.1259/bjr.20221087.
43. Tumor Enhancement on Dynamic CT: A Predictive Factor for Recurrence After Nephrectomy in Localized T1 Clear Cell Renal Cell Carcinoma. *Anticancer Res.* **2018**, *38*, doi:10.21873/anticanres.12486.
44. Lee-Felker, S.A.; Felker, E.R.; Tan, N.; Margolis, D.J.A.; Young, J.R.; Sayre, J.; Raman, S.S. Qualitative and Quantitative MDCT Features for Differentiating Clear Cell Renal Cell Carcinoma From Other Solid Renal Cortical Masses. *Am. J. Roentgenol.* **2014**, *203*, W516–W524, doi:10.2214/AJR.14.12460.
45. Luo, S.; Lin, W.; Wu, J.; Zhang, W.; Kui, X.; Lai, S.; Wei, R.; Pang, X.; Wang, Y.; He, C.; et al. Quantitative Measurement on Contrast-Enhanced CT Distinguishes Small Clear Cell Renal Cell Carcinoma From Benign Renal Tumors: A Multicenter Study. *Acad. Radiol.* **2024**, *31*, 1460–1471, doi:10.1016/j.acra.2023.10.014.
46. Zhu, Q.; Zou, J.; Ye, J.; Zhu, W.; Wu, J.; Chen, W. Comparative Study of Conventional ROI-Based and Volumetric Histogram Analysis Derived from CT Enhancement in Differentiating Malignant and Benign Renal Tumors. *Br. J. Radiol.* **2022**, *95*, 20210801, doi:10.1259/bjr.20210801.

 doi:10.20944/preprints202605.0012.v1

47. Yi, X.; Xiao, Q.; Zeng, F.; Yin, H.; Li, Z.; Qian, C.; Wang, C.; Lei, G.; Xu, Q.; Li, C.; et al. Computed Tomography Radiomics for Predicting Pathological Grade of Renal Cell Carcinoma. *Front. Oncol.* **2021**, *10*, 570396, doi:10.3389/fonc.2020.570396.
48. Al Nasibi, K.; Pickovsky, J.S.; Eldehimi, F.; Flood, T.A.; Lavallee, L.T.; Tsampalieros, A.K.; Schieda, N. Development of a Multiparametric Renal CT Algorithm for Diagnosis of Clear Cell Renal Cell Carcinoma Among Small (≤ 4 Cm) Solid Renal Masses. *Am. J. Roentgenol.* **2022**, *219*, 814–823, doi:10.2214/AJR.22.27971.
49. Zhang, X.; Zhang, G.; Xu, L.; Bai, X.; Zhang, J.; Chen, L.; Lu, X.; Yu, S.; Jin, Z.; Sun, H. Prediction of World Health Organization /International Society of Urological Pathology (WHO/ISUP) Pathological Grading of Clear Cell Renal Cell Carcinoma by Dual-Layer Spectral CT. *Acad. Radiol.* **2023**, *30*, 2321–2328, doi:10.1016/j.acra.2022.12.002.
50. Posada Calderon, L.P.; Eismann, L.; Reese, S.W.; Reznik, E.; Hakimi, A.A. Advances in Imaging-Based Biomarkers in Renal Cell Carcinoma: A Critical Analysis of the Current Literature. *Cancers* **2023**, *15*, 354, doi:10.3390/cancers15020354.
51. Rogers, W.; Thulasi Seetha, S.; Refaee, T.A.G.; Lieverse, R.I.Y.; Granzier, R.W.Y.; Ibrahim, A.; Keek, S.A.; Sanduleanu, S.; Primakov, S.P.; Beuque, M.P.L.; et al. Radiomics: From Qualitative to Quantitative Imaging. *Br. J. Radiol.* **2020**, *93*, 20190948, doi:10.1259/bjr.20190948.
52. Lafata, K.J.; Wang, Y.; Konkel, B.; Yin, F.-F.; Bashir, M.R. Radiomics: A Primer on High-Throughput Image Phenotyping. *Abdom. Radiol.* **2021**, *47*, 2986–3002, doi:10.1007/s00261-021-03254-x.
53. McCague, C.; Ramlee, S.; Reinius, M.; Selby, I.; Hulse, D.; Piyatissa, P.; Bura, V.; Crispin-Ortuzar, M.; Sala, E.; Woitek, R. Introduction to Radiomics for a Clinical Audience. *Clin. Radiol.* **2023**, *78*, 83–98, doi:10.1016/j.crad.2022.08.149.
54. Shur, J.D.; Doran, S.J.; Kumar, S.; Ap Dafydd, D.; Downey, K.; O'Connor, J.P.B.; Papanikolaou, N.; Messiou, C.; Koh, D.-M.; Orton, M.R. Radiomics in Oncology: A Practical Guide. *RadioGraphics* **2021**, *41*, 1717–1732, doi:10.1148/rg.2021210037.
55. Zhang, X.; Zhang, Y.; Zhang, G.; Qiu, X.; Tan, W.; Yin, X.; Liao, L. Deep Learning With Radiomics for Disease Diagnosis and Treatment: Challenges and Potential. *Front. Oncol.* **2022**, *12*, 773840, doi:10.3389/fonc.2022.773840.
56. Aerts, H.J.W.L. The Potential of Radiomic-Based Phenotyping in Precision Medicine: A Review. *JAMA Oncol.* **2016**, *2*, 1636, doi:10.1001/jamaoncol.2016.2631.
57. Abbasian Ardakani, A.; Bureau, N.J.; Ciaccio, E.J.; Acharya, U.R. Interpretation of Radiomics Features–A Pictorial Review. *Comput. Methods Programs Biomed.* **2022**, *215*, 106609, doi:10.1016/j.cmpb.2021.106609.
58. Avanzo, M.; Wei, L.; Stancanello, J.; Vallières, M.; Rao, A.; Morin, O.; Mattonen, S.A.; El Naqa, I. Machine and Deep Learning Methods for Radiomics. *Med. Phys.* **2020**, *47*, doi:10.1002/mp.13678.
59. Zwanenburg, A.; Vallières, M.; Abdalah, M.A.; Aerts, H.J.W.L.; Andrearczyk, V.; Apte, A.; Ashrafinia, S.; Bakas, S.; Beukinga, R.J.; Boellaard, R.; et al. The Image Biomarker Standardization Initiative: Standardized Quantitative Radiomics for High-Throughput Image-Based Phenotyping. *Radiology* **2020**, *295*, 328–338, doi:10.1148/radiol.2020191145.
60. Caruso, D.; Polici, M.; Zerunian, M.; Pucciarelli, F.; Guido, G.; Polidori, T.; Landolfi, F.; Nicolai, M.; Lucertini, E.; Tarallo, M.; et al. Radiomics in Oncology, Part 2: Thoracic, Genito-Urinary, Breast, Neurological, Hematologic and Musculoskeletal Applications. *Cancers* **2021**, *13*, 2681, doi:10.3390/cancers13112681.
61. Liu, X.; Elbanan, M.G.; Luna, A.; Haider, M.A.; Smith, A.D.; Sabottke, C.F.; Spieler, B.M.; Turkbey, B.; Fuentes, D.; Moawad, A.; et al. Radiomics in Abdominopelvic Solid-Organ Oncologic Imaging: Current Status. *Am. J. Roentgenol.* **2022**, *219*, 985–995, doi:10.2214/AJR.22.27695.
62. Ferro, A.; Bottosso, M.; Dieci, M.V.; Scagliori, E.; Miglietta, F.; Aldegheri, V.; Bonanno, L.; Caumo, F.; Guarneri, V.; Griguolo, G.; et al. Clinical Applications of Radiomics and Deep Learning in Breast and Lung Cancer: A Narrative Literature Review on Current Evidence and Future Perspectives. *Crit. Rev. Oncol. Hematol.* **2024**, *203*, 104479, doi:10.1016/j.critrevonc.2024.104479.
63. Uhlig, A.; Uhlig, J.; Leha, A.; Biggemann, L.; Bachanek, S.; Stöckle, M.; Reichert, M.; Lotz, J.; Zeuschner, P.; Maßmann, A. Radiomics and Machine Learning for Renal Tumor Subtype Assessment Using Multiphase Computed Tomography in a Multicenter Setting. *Eur. Radiol.* **2024**, *34*, 6254–6263, doi:10.1007/s00330-024-10731-6.

 doi:10.20944/preprints202605.0012.v1

64. Bhandari, A.; Ibrahim, M.; Sharma, C.; Liong, R.; Gustafson, S.; Prior, M. CT-Based Radiomics for Differentiating Renal Tumours: A Systematic Review. *Abdom. Radiol.* **2021**, *46*, 2052–2063, doi:10.1007/s00261-020-02832-9.
65. Dehghani Firouzabadi, F.; Gopal, N.; Homayounieh, F.; Anari, P.Y.; Li, X.; Ball, M.W.; Jones, E.C.; Samimi, S.; Turkbey, E.; Malayeri, A.A. CT Radiomics for Differentiating Oncocytoma from Renal Cell Carcinomas: Systematic Review and Meta-Analysis. *Clin. Imaging* **2023**, *94*, 9–17, doi:10.1016/j.clinimag.2022.11.007.
66. Lv, D.; Liu, R.; Wang, X.; Liang, T.; Zhang, L.; Zeng, W.; He, Z.; Deng, L.; Zhang, Z.; Qin, G.; et al. A Comprehensive Multi-Task Deep Learning Model for Kidney Cancer: Histological Subtyping, Clinical Staging, and Anatomical Complexity Grading. *Eur. Radiol.* **2026**, doi:10.1007/s00330-026-12322-z.
67. Li, X.; Ma, Q.; Nie, P.; Zheng, Y.; Dong, C.; Xu, W. A CT-Based Radiomics Nomogram for Differentiation of Renal Oncocytoma and Chromophobe Renal Cell Carcinoma with a Central Scar-Matched Study. *Br. J. Radiol.* **2022**, *95*, 20210534, doi:10.1259/bjr.20210534.
68. Yu, Z.; Ding, J.; Pang, H.; Fang, H.; He, F.; Xu, C.; Li, X.; Ren, K. A Triple-Classification for Differentiating Renal Oncocytoma from Renal Cell Carcinoma Subtypes and CK7 Expression Evaluation: A Radiomics Analysis. *BMC Urol.* **2022**, *22*, 147, doi:10.1186/s12894-022-01099-0.
69. Mühlbauer, J.; Egen, L.; Kowalewski, K.-F.; Grilli, M.; Walach, M.T.; Westhoff, N.; Nuhn, P.; Laqua, F.C.; Baessler, B.; Kriegmair, M.C. Radiomics in Renal Cell Carcinoma—A Systematic Review and Meta-Analysis. *Cancers* **2021**, *13*, 1348, doi:10.3390/cancers13061348.
70. Jaggi, A.; Mastrodicasa, D.; Charville, G.W.; Jeffrey, R.B.; Napel, S.; Patel, B. Quantitative Image Features from Radiomic Biopsy Differentiate Oncocytoma from Chromophobe Renal Cell Carcinoma. *J. Med. Imaging* **2021**, *8*, doi:10.1117/1.JMI.8.5.054501.
71. Lomer, N.B.; Abdi, S.; Ashoobi, M.A.; Ahmadzadeh, A.M.; Ghasemi, A.; Torigian, D.A. Accuracy of CT-Based Radiomics Models for Preoperative Grading of Clear Cell Renal Cell Carcinoma: A Systematic Review and Meta-Analysis. *Acad. Radiol.* **2025**, *32*, 6664–6676, doi:10.1016/j.acra.2025.05.049.
72. Broomand Lomer, N.; Ghasemi, A.; Ahmadzadeh, A.M.; A. Torigian, D. MRI-Based Radiomics for Differentiating High-Grade from Low-Grade Clear Cell Renal Cell Carcinoma: A Systematic Review and Meta-Analysis. *Abdom. Radiol.* **2025**, *50*, 5852–5871, doi:10.1007/s00261-025-04982-0.
73. Meng, X.; Shu, J.; Xia, Y.; Yang, R. A CT-Based Radiomics Approach for the Differential Diagnosis of Sarcomatoid and Clear Cell Renal Cell Carcinoma. *BioMed Res. Int.* **2020**, *2020*, 7103647, doi:10.1155/2020/7103647.
74. Gurbani, S.; Morgan, D.; Jog, V.; Dreyfuss, L.; Shen, M.; Das, A.; Abel, E.J.; Lubner, M.G. Evaluation of Radiomics and Machine Learning in Identification of Aggressive Tumor Features in Renal Cell Carcinoma (RCC). *Abdom. Radiol.* **2021**, *46*, 4278–4288, doi:10.1007/s00261-021-03083-y.
75. Xu, J.; Gao, S.; Zhu, Q.; Dai, F.; Sun, C.; Lee, W.; Ye, Y.; Deng, G.; Huang, Z.; Li, X.; et al. Machine Learning-Based Multiparametric CT Radiomics for Predicting Microvascular Invasion before Nephrectomy in Clear Cell Renal Cell Carcinoma. *Abdom. Radiol.* **2025**, *50*, 5263–5273, doi:10.1007/s00261-025-04956-2.
76. Khene, Z.-E.; Bhanvadia, R.; Tachibana, I.; Sharma, P.; Graber, W.; Bertail, T.; Fleury, R.; De Crevoisier, R.; Bensalah, K.; Lotan, Y.; et al. Predicting Recurrence After Surgical Resection for High-Risk Localized Renal Cell Carcinoma: A Radiomics Clinical Integration Approach. *J. Urol.* **2025**, *214*, 296–307, doi:10.1097/JU.0000000000004588.
77. Xing, J.; Liu, Y.; Wang, Z.; Xu, A.; Su, S.; Shen, S.; Wang, Z. Incremental Value of Radiomics with Machine Learning to the Existing Prognostic Models for Predicting Outcome in Renal Cell Carcinoma. *Front. Oncol.* **2023**, *13*, 1036734, doi:10.3389/fonc.2023.1036734.
78. Feng, Z.; Yang, P.; Wu, Y.; Li, Z.; Hu, Z.; Lan, W. Radiomics-Based Tumor Heterogeneity Augments Clinicopathological Models for Predicting Recurrence in High-Risk Clear Cell Renal Cell Carcinoma after Nephrectomy. *Abdom. Radiol.* **2025**, doi:10.1007/s00261-025-05108-2.
79. Tang, X.; Pang, T.; Yan, W.; Qian, W.; Gong, Y.; Yang, Z. The Prognostic Value of Radiomics Features Extracted From Computed Tomography in Patients With Localized Clear Cell Renal Cell Carcinoma After Nephrectomy. *Front. Oncol.* **2021**, *11*, 591502, doi:10.3389/fonc.2021.591502.

 doi:10.20944/preprints202605.0012.v1

80. Khodabakhshi, Z.; Amini, M.; Mostafaei, S.; Haddadi Avval, A.; Nazari, M.; Oveisi, M.; Shiri, I.; Zaidi, H. Overall Survival Prediction in Renal Cell Carcinoma Patients Using Computed Tomography Radiomic and Clinical Information. *J. Digit. Imaging* **2021**, *34*, 1086–1098, doi:10.1007/s10278-021-00500-y.
81. Lu, Z.; Wu, S.; Ni, D.; Zhou, M.; Wang, T.; Zhou, X.; Huang, L.; Yan, Y. Survival Analysis of Clear Cell Renal Cell Carcinoma Based on Radiomics and Deep Learning Features from CT Images. *Medicine (Baltimore)* **2024**, *103*, e40723, doi:10.1097/MD.0000000000040723.
82. Rossi, E.; Boldrini, L.; Maratta, M.G.; Gatta, R.; Votta, C.; Tortora, G.; Schinzari, G. Radiomics to Predict Immunotherapy Efficacy in Advanced Renal Cell Carcinoma: A Retrospective Study. *Hum. Vaccines Immunother.* **2023**, *19*, 2172926, doi:10.1080/21645515.2023.2172926.
83. Reese, S.W.; Barbakoff, D.; Ucpinar, B.A.; Knezevic, A.; Fitzgerald, K.; Eismann, L.; Tehrani, Y.M.; Arroyave, J.S.; Khaleel, S.; Khandwala, Y.S.; et al. Radiomic Biomarkers Associated with Immune Checkpoint Blockade Response for Advanced Renal Cell Carcinoma. *Urol. Oncol. Semin. Orig. Investig.* **2025**, *43*, 708.e15-708.e24, doi:10.1016/j.urolonc.2025.08.012.
84. Sun, R.; Limkin, E.J.; Vakalopoulou, M.; Dercle, L.; Champiat, S.; Han, S.R.; Verlingue, L.; Brandao, D.; Lancia, A.; Ammari, S.; et al. A Radiomics Approach to Assess Tumour-Infiltrating CD8 Cells and Response to Anti-PD-1 or Anti-PD-L1 Immunotherapy: An Imaging Biomarker, Retrospective Multicohort Study. *Lancet Oncol.* **2018**, *19*, 1180–1191, doi:10.1016/S1470-2045(18)30413-3.
85. Zhang, C.; De A. F. Fonseca, L.; Shi, Z.; Zhu, C.; Dekker, A.; Bermejo, I.; Wee, L. Systematic Review of Radiomic Biomarkers for Predicting Immune Checkpoint Inhibitor Treatment Outcomes. *Methods* **2021**, *188*, 61–72, doi:10.1016/j.ymeth.2020.11.005.
86. Khene, Z.-E.; Tachibana, I.; Bertail, T.; Fleury, R.; Bhanvadia, R.; Kapur, P.; Rajaram, S.; Guo, J.; Christie, A.; Pedrosa, I.; et al. Clinical Application of Radiomics for the Prediction of Treatment Outcome and Survival in Patients with Renal Cell Carcinoma: A Systematic Review. *World J. Urol.* **2024**, *42*, 541, doi:10.1007/s00345-024-05247-z.
87. Kocak, B.; Durmaz, E.S.; Erdim, C.; Ates, E.; Kaya, O.K.; Kilickesmez, O. Radiomics of Renal Masses: Systematic Review of Reproducibility and Validation Strategies. *Am. J. Roentgenol.* **2020**, *214*, 129–136, doi:10.2214/AJR.19.21709.
88. Ursprung, S.; Beer, L.; Bruining, A.; Woitek, R.; Stewart, G.D.; Gallagher, F.A.; Sala, E. Radiomics of Computed Tomography and Magnetic Resonance Imaging in Renal Cell Carcinoma—a Systematic Review and Meta-Analysis. *Eur. Radiol.* **2020**, *30*, 3558–3566, doi:10.1007/s00330-020-06666-3.
89. Shehata, M.; Abouelkheir, R.T.; Gayhart, M.; Van Bogaert, E.; Abou El-Ghar, M.; Dwyer, A.C.; Ouseph, R.; Yousaf, J.; Ghazal, M.; Contractor, S.; et al. Role of AI and Radiomic Markers in Early Diagnosis of Renal Cancer and Clinical Outcome Prediction: A Brief Review. *Cancers* **2023**, *15*, 2835, doi:10.3390/cancers15102835.